*Annual Review of Fluid Mechanics*

# Bluff Bodies and Wake–Wall Interactions

Mark C. Thompson,[1] Thomas Leweke,[2] and Kerry Hourigan[1]

[1]Department of Mechanical & Aerospace Engineering, Monash University, Clayton, VIC 3800, Australia; email: mark.thompson@monash.edu

[2]IRPHE (Institut de Recherche sur les Phénomènes Hors Equilibre), CNRS, Aix-Marseille Université, Centrale Marseille, 13384 Marseille, France





Annu. Rev. Fluid Mech. 2021. 53:347–76

First published as a Review in Advance on October 5, 2020

The *Annual Review of Fluid Mechanics* is online at fluid.annualreviews.org

https://doi.org/10.1146/annurev-fluid-072220-123637



## Keywords

bluff bodies, wall interactions, wake transitions, flow stability, solid–solid contact

## Abstract

This review surveys the dramatic variations in wake structures and flow transitions, in addition to body forces, that appear as the motion of bluff bodies through a fluid occurs increasingly closer to a solid wall. In particular, we discuss the two cases of bluff bodies translating parallel to solid walls at varying heights and bluff bodies impacting on solid walls. In the former case, we highlight the changes to the wake structures as the flow varies from that of an isolated body to that of a body on or very close to the wall, including the effects when the body is rotating. For the latter case of an impacting body, we review the flow structures following impact and their transition to three-dimensionality. We discuss the issue of whether there is solid–solid contact between the bluff body and a wall and its importance to body motion.

## 1. INTRODUCTION

The flow around generic bluff bodies, such as circular cylinders and spheres, has been studied for more than a century. The vortex-shedding phenomenon occurring in the wake of these bodies and the associated fluid–structure interactions have been the topic of several previous contributions to the *Annual Review of Fluid Mechanics*: Berger & Wille (1972), Bearman (1984), Oertel (1990), Williamson (1996b), Williamson & Govardhan (2004), Choi et al. (2008), and Ern et al. (2012).

Building on and extending these reviews, this article focuses on the wake dynamics of generic bluff bodies when moving relative to, and interacting with, walls in an otherwise quiescent fluid. Examples of the wakes generated by a cylinder rolling on a wall and a sphere impacting a wall are shown in **Figure 1**. These vortical flows bear little resemblance to the wakes of isolated cylinders and spheres in freestream.

### 1.1. Practical Significance

A solid body moving along or colliding with a solid surface is a common element relevant to many industrial and environmental processes, leading to complex energy exchanges. An example is the resuspension of particles deposited on a surface, such as dust on the ground or sediments in rivers, by the wake generated by the impact of an object or other particles; see, e.g., Willetts (1998) and Ziskind (2006) for reviews on this topic (also see **Figure 1*b***). Wear due to particle impacts on surfaces is a major problem in many areas, including pumping and processing of slurry flows (Clark 1992), as is the damaging impact of small particles on high-technology equipment in desert environments (Yildirim et al. 2017). Micrometer-scale solid particles are used in a range of processes in industries such as metallurgy and pharmaceutical manufacturing, including polishing, shot peening, sand blasting, and kinetic consolidation processes. At a larger scale, many sports, such as football, cricket, baseball, snooker, pétanque, bowls, tennis and table tennis, and golf, to name but a few, involve bluff bodies that move near and on a surface and where impact, rolling, spin, and bounce are important.

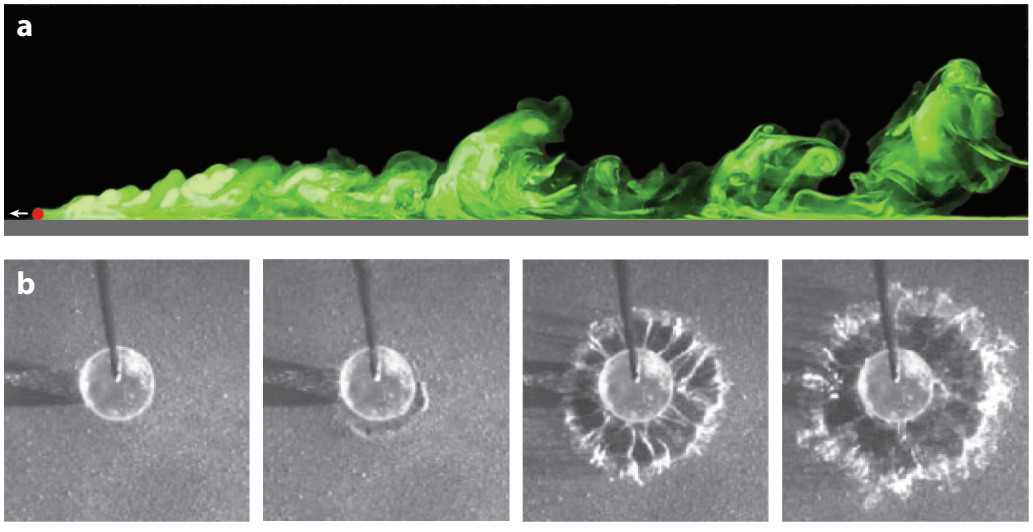


**Figure 1**

(*a*) Mixing induced by a cylinder (*red circle*) rolling in a quiescent fluid along a wall previously coated with a thin layer of dyed fluid. Experimental visualization in water at $Re = 220$. (*b*) Resuspension of a layer of particles by the normal wall impact of a sphere at $Re = 3{,}100$. Oblique view from above. Panel *b* reprinted with permission from Eames & Dalziel (1999), copyright 1999 AIP Publishing.

## 1.2. The Problem of Solid-to-Solid Contact

Sisyphus, according to Greek mythology, was condemned to eternally repeat the process of rolling a massive boulder up a hill, only for it to then roll down the hill again. Were we to model this process by a perfectly smooth sphere and hill within an incompressible Newtonian atmosphere, a startling result would await—no matter how mightily Sisyphus may strain, the sphere would not budge, even on a steep slope, due to infinite resistive pressure forces near the point of contact. This is the so-called rolling paradox (see Section 4.3). However, of course bodies do roll, with the first scientific study initially published in 1638 by Galileo with his famous rolling-sphere experiments [Galilei 1914 (1638)].

Galileo was reputed, anecdotally, to have dropped spheres from the Tower of Pisa to show that acceleration was proportional to gravitational force, independent of mass. However, for a perfectly smooth ball and ground and an incompressible Newtonian atmosphere, the dropped spheres would never actually touch the ground, due to the infinite fluid forces in the small gap as the sphere approaches the solid surface (Brenner 1961). And yet solid-to-solid impacts of dropped bodies are evidently observed (and heard).

When isolated from a wall, the identical assumptions for a body moving relative to a fluid do allow for accurate modeling of the body and its wake (e.g., Johnson & Patel 1999, Thompson et al. 1996). Therein lies a major challenge to understanding the seemingly simple problem of a body in a fluid moving near, or impacting on, a wall.

## 1.3. Scope of the Review

This review focuses on the flow around the generic bluff bodies of a circular cylinder and a sphere, showing how the characteristics of the wake change due to the presence of the wall under a variety of translation, rotation, rolling, and impact conditions, as well as the effects of Reynolds number—see **Figure 2** for the setups and important parameters. At present, the results of past investigations are often scattered throughout various research subfields, not always cross-referenced and sometimes inaccurate. This review aims to provide an overview of these various studies, raising important questions still to be fully addressed. The focus is on bodies translating in otherwise stationary fluids with fixed walls. The issue of fluid–structure interaction, and specifically flow-induced vibration, is limited to a brief discussion concerning freely rolling bodies. Most of the referenced results were obtained from experiments in water channels or tanks, or in computational studies involving direct numerical simulations. Comparisons between the two are shown where possible.

In order to provide some context, we start with a brief review of the wake transitions of generic bluff bodies—two-dimensional (2D) cylinders and 3D spheres—at significant distances from a wall, considering both nonrotating and rotating cases, as well as impulsively arrested bodies. Then, we map the changes in wakes as the bodies are located increasingly closer to a wall. Finally, we review the issues of bluff-body contact with a wall and point out future directions on this topic.

# 2. UNIFORMLY TRANSLATING ISOLATED BLUFF BODIES

## 2.1. Nonrotating Bodies

The flow past nonrotating cylinders and spheres has been a generic fluid flow problem of continuing interest for more than a century, and the intricate experimental and mathematical details of the transitions leading toward a fully turbulent wake have been revealed especially over the last three decades.

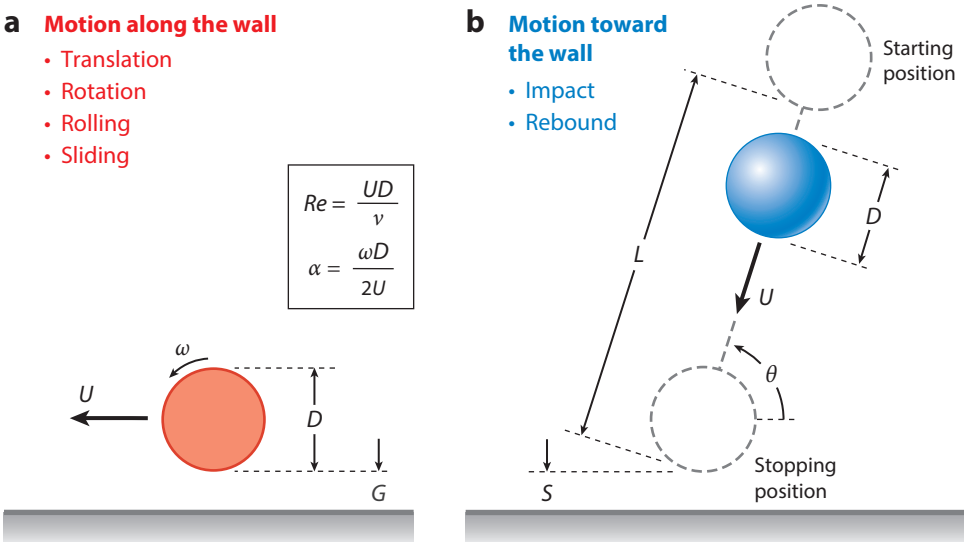


**Figure 2**

The two types of configurations considered in this review, including the main parameters: (*a*) a bluff body translating and rotating along a wall, separated by a gap $G$; and (*b*) a body, initially at rest, moving a distance $L$ before stopping at or near a wall (without or with rebound). In all cases the fluid is stationary with respect to the wall.

**2.1.1. Circular cylinders.** The initial transition for a cylinder occurs at Reynolds number $Re_{C_1} \approx 46$ through a Hopf bifurcation from a symmetric pair of attached recirculation bubbles to a periodic 2D Bénard–von Kármán (BvK) wake (see **Figure 3*a***) (Williamson 1989, Dušek et al. 1994). Here, the Reynolds number is based on the freestream velocity ($U$) and the cylinder diameter ($D$): $Re = UD/\nu$ ($\nu$ is the kinematic viscosity of the fluid). Upon increase of the Reynolds number, the wake next undergoes a subcritical (hysteretic) 3D transition at $Re_{C_2} \approx 190$ (Barkley & Henderson 1996; Williamson 1996a,b), which manifests as a sinusoidal distortion of the spanwise vortex rollers with streamwise vortex structures connecting these. At onset, the spanwise wavelength ($\lambda$) is approximately four cylinder diameters, and this wake instability is commonly known as mode A. Upon further increase of the Reynolds number, another 3D mode of much shorter spanwise wavelength ($\lambda \approx D$), mode B, becomes unstable at $Re_{C_3} \approx 260$. The remnants of this mode appear to persist at much higher Reynolds numbers after the wake becomes fully chaotic (Williamson 1996a,b; Henderson 1997). The characteristic 3D modes are visualized in **Figure 3*b***. Of interest, equivalent modes have also been recognized in the wakes of other 2D cylindrical bodies, such as square cylinders (Robichaux et al. 1999) and angled airfoils (He et al. 2017). However, different modes can be important for other cylindrical geometries; e.g., a quasi-periodic mode is the first transition mode of a normal-flat-plate wake (Thompson et al. 2006b). When the flow is artificially held steady for $Re > Re_{C_1}$, a steady 3D perturbation develops for $Re \geq 100$ that resembles the mode E instability occurring naturally when the cylinder rotates at high rates (see **Figure 4*a***).

**Hopf bifurcation:** loss of stability of a steady state, giving rise to a periodic solution, as the control parameter is increased

**2.1.2. Spheres.** The sequence of wake modes for a sphere, as $Re$ is increased, is illustrated in **Figure 3*c***. Consistent with other studies (Ghidersa & Dušek 2000, Tomboulides & Orszag 2000, Thompson et al. 2001), experiments and numerical computations performed by Johnson & Patel (1999) found that the initial axisymmetric wake undergoes a regular bifurcation through an

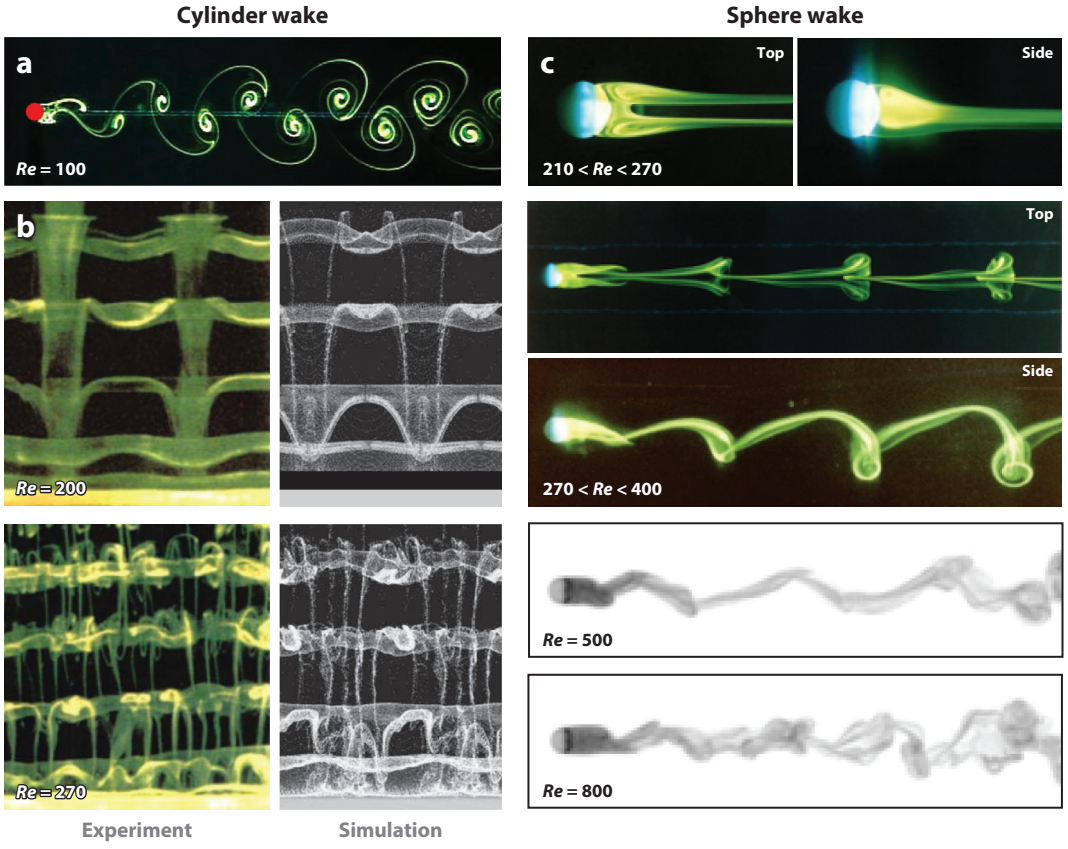


**Figure 3**

(*a*) Two-dimensional (2D) periodic cylinder wake (experimental dye visualization). (*b*) 3D structures in the wake of a cylinder (flow is upward, and the cylinder is at the bottom). (*Top row*) Mode A; (*bottom row*) mode B; (*left column*) dye visualization; (*right column*) numerical simulation with tracer particles. Panel *b* adapted with permission from (*left column*) Williamson (1996a), copyright 1996 Cambridge University Press; and (*right column*) Thompson et al. (2006b), copyright 2006 Elsevier. (*c*) Evolution of the wake of a sphere with increasing Reynolds number (dye visualization and numerical simulation). Experimental top views in panel *c* reprinted with permission from Thompson et al. (2001), copyright 2001 Elsevier.



off-axis shift of the steady recirculating bubble at $Re_{S_1} \approx 210$. This results in a double-threaded wake consisting of a trailing vortex pair, as observed previously for buoyant oil drops (Magarvey & Bishop 1961a,b). Upon further increase of $Re$, a second topological transition from the steady two-threaded wake to a periodic wake occurs at $Re_{S_2} \approx 270$ (above references), with the trailing vortices forming kinks that develop into strongly skewed loops advecting downstream. Computations by Mittal (1999) and experiments of Brücker (2001) showed that the vortex loops in the wake lose planar symmetry at $Re_{S_3} \approx 400$. These vortex loops are maintained at much higher Reynolds numbers, despite an increasing chaotic component. Through large-eddy simulations, Chomaz et al. (1993) and Tomboulides & Orszag (2000) reported fine-scale wake flow structures for $500 < Re < 1{,}000$; they speculated that these develop from a Kelvin–Helmholtz instability of the shear layer separating from the sphere. In agreement, Magarvey & Bishop (1961b) experimentally observed a breakdown in periodicity of the hairpin shedding for $Re > 600$. The same shear layer instability manifests in a cylinder wake beyond $Re \approx 2{,}000$ (see, e.g., Prasad & Williamson

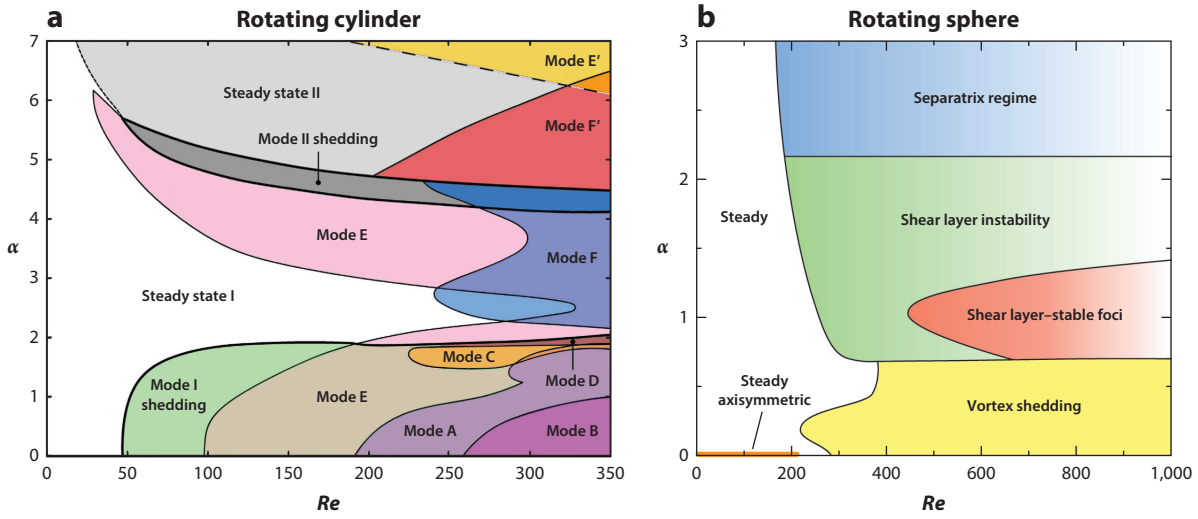


**Figure 4**

(*a*) Stability diagram for a cylinder rotating at rate $\alpha = \omega D/(2U)$. Panel *a* adapted with permission from Rao et al. (2015a), copyright 2015 Elsevier. (*b*) Wake regimes of a rotating sphere, as function of *Re* and $\alpha$, based on data collected by Poon et al. (2014) and Dobson et al. (2014).



1997, Thompson & Hourigan 2005), although, for experiments at least, the onset is dependent on background turbulence.

## 2.2. Rotating Bodies

The addition of a body rotation around an axis perpendicular to the flow direction breaks the symmetry of the configuration and leads to changes in the wake characteristics and transition behavior. For these cases, a nondimensional rotation rate $\alpha$ can be defined, given by the ratio of the circumferential speed of the cylinder surface and the flow velocity or, equivalently, the cylinder translation speed: $\alpha = \omega D/(2U)$, with $\omega$ the angular velocity of the body (**Figure 2*a***).

**2.2.1. Circular cylinders.** Numerical and experimental investigations have characterized and quantified the wake of a rotating cylinder for rotation rates $\alpha \leq 7$ and Reynolds numbers $Re \leq 400$ (see **Figure 4*a***). Various 2D and 3D transitions have been identified and mapped using linear stability analysis. This effectively extends the previously described results for a nonrotating cylinder (Section 2.1.1) from the $\alpha = 0$ axis into the $Re$–$\alpha$ parameter space. For small rotation rates ($\alpha \lesssim 2$), the rotation breaks the symmetry of the BvK wake but essentially only perturbs the vortex shedding and transition modes (A and B). However, as the rotation rate approaches $\alpha = 2$, the connection points at the cylinder of the upstream and downstream stagnation streamlines essentially merge, significantly altering the flow topology so that shedding is increasingly suppressed. At even higher rotation rates, these two streamlines join and separate from the surface of the cylinder, forming a closed region of pure rotation about the cylinder. Given this change to the underlying base flow with $\alpha$, the parameter space can be broadly split into two regions, $\alpha < 2$ and $\alpha > 2$, as the parameter map of **Figure 4*a*** shows. Two unsteady 2D regimes exist: Mode I shedding occurs for $\alpha \lesssim 2$ and is characterized by alternate vortex shedding, while mode II shedding only occurs over a small range of $\alpha$, at much higher rotation rates that result in single-sided vortex shedding

(see, e.g., Stojković et al. 2002, 2003; Mittal & Kumar 2003). Two steady flow regimes have also been identified (Mittal & Kumar 2003, Pralits et al. 2010, Rao et al. 2015a): Steady state I occurs at lower *Re*, while steady state II manifests at higher rotation rates beyond the mode II shedding region. These two states are distinguished by differences in flow features, such as the drag coefficient and the location of stagnation points. At higher *Re*, a variety of unstable 3D modes with different spanwise wavelengths are found, including a periodic subharmonic mode (C), which is also found in other asymmetric bluff body flow configurations, such as curved circular cylinders (rings) or inclined square cylinders (Sheard et al. 2005, Sheard 2011), as well as a steady 3D mode (E).

**2.2.2. Spheres.** Previous numerical investigations (Giacobello et al. 2009, Kim 2009, Dobson et al. 2014, Poon et al. 2014, Rajamuni et al. 2018) of the effects of rotation on the wakes of rigidly mounted spheres at low Reynolds numbers ($Re \leq 1{,}000$) have revealed considerable wake modifications and even suppression of the vortex shedding, depending on rotation rate. In comparison with the cylinder case, the wake structure is more strongly affected at lower rotation rates, with **Figure 4*b*** showing that a broad change occurs beyond $\alpha \simeq 0.7$. Similar to the cylinder, in the rotation centerplane, high rotation causes the streamlines to bend around the sphere, again leading to an isolated region of corotation near the sphere surface (separatrix regime).

## 2.3. Impulsively Arrested Bodies

The flow evolution associated with a bluff body impulsively stopping in an unbounded fluid has received little attention to date.

**2.3.1. Circular cylinders.** For the case of an arresting cylinder, Tatsuno & Taneda (1971), Wang & Dalton (1991), and Sheard et al. (2007) showed that, during cylinder motion, a recirculating wake develops and grows behind the body, consisting of an attached counter-rotating vortex pair. After the cylinder is impulsively stopped, the momentum in the surrounding fluid carries the wake over the cylinder, and the shear at the surface induces secondary vortices that pair with the primary wake vortices as the latter pass the cylinder (**Figure 5*a***). In the subsequent flow evolution, Sheard et al. (2007) found that, similar to the flow past an arresting sphere discussed below, these counter-rotating vortex pairs self-propel over a range of sometimes surprising trajectories. For low Reynolds numbers and short translation distances, the wake vortices move past the cylinder and continue in the direction of the original cylinder motion. For higher Reynolds numbers, the pairs deviate outward in circular arcs of increasing curvature, even to the extent that they can actually collide behind the cylinder. The curvature depends on the circulation balance of the vortex pairs. At sufficiently large translation distances, a wake instability that would lead to vortex shedding breaks the reflective symmetry about the centerline of the wake.

**2.3.2. Spheres.** Leweke et al. (2004b) and Thompson et al. (2007) have investigated the flow dynamics of an impulsively arrested sphere. For an arrest occurring in isolation (**Figure 5*b***), the recirculating wake translates toward the arrested sphere before spreading laterally as a vortex ring in the original upstream direction. A second vortex ring of opposite sign is induced from the sphere surface and pairs with the primary ring. The vortex ring pair follows a loop trajectory due to mutual induction, after which the primary ring continues its upstream motion, whereas the secondary ring is left behind and fades out.

**Subharmonic:** having half the frequency of the base flow

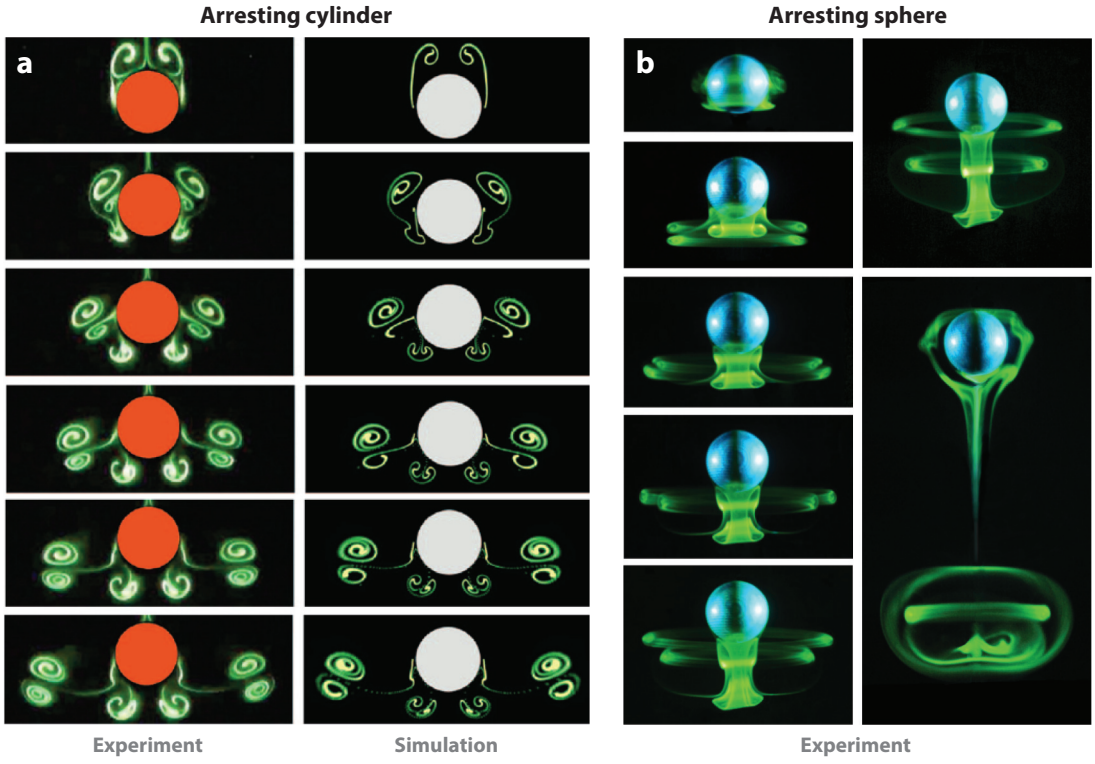


**Figure 5**

(*a*) Flow around an impulsively arrested cylinder of diameter $D$ previously translating a distance $2D$ from top to bottom at $Re = 500$; experimental dye visualization (*left*) and numerical simulation with tracer particles (*right*). Panel *a* adapted with permission from Sheard et al. (2007), copyright 2007 AIP Publishing. (*b*) Experimental dye visualization of the vortex rings developing for an impulsively arrested sphere after translating a distance $5D$ at $Re = 800$.



## 3. BLUFF BODIES MOVING PARALLEL TO A WALL

### 3.1. Circular Cylinders

Taneda (1965) was one of the first to visualize the wake of a circular cylinder moving parallel to a wall. He specifically examined the change to the vortex street as the gap height was reduced from $G/D = 0.6$ to 0.1 (see **Figure 2*a***) at $Re = 170$. For the smaller gap, it appeared that only a single row of vortices formed on the side of the cylinder opposite from the wall, with the individual vortices being unstable and decaying rapidly. The streamwise wavelength of the vortex street increased as the gap was reduced.

Various authors have since investigated the effect of wall proximity at low Reynolds numbers through 2D numerical simulations. For example, for nonrotating cylinders, Huang & Sung (2007) quantified the wake and forces for $0.1 \leq G/D \leq 1$ and for $Re \leq 600$, while Yoon et al. (2010) considered the effect of gap height at $Re = 200$. A change from the standard BvK wake to a wake dominated by one-sided shedding was found to occur at $G/D \approx 0.25$. Also, the shedding frequency, $f$, expressed as the nondimensional Strouhal number, $St = fD/U$, initially increases slightly as the gap is reduced toward $G/D = 0.5$, but it decreases rapidly beyond this point, which is consistent with Taneda's (1965) observation of an increased wavelength. The higher blockage to fluid passing under the cylinder, as the wall gap is reduced, tends to stabilize the wake to the onset of periodic

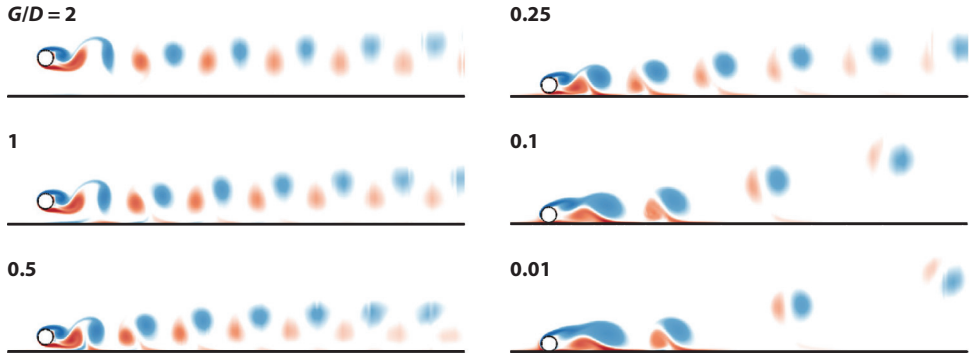


**Figure 6**

Two-dimensional wakes (vorticity fields) of cylinders of diameter $D$ translating parallel to a solid wall at different gaps $G$, for $Re = 200$. Figure adapted with permission from Rao et al. (2013), copyright 2013 Elsevier.



shedding, resulting in an increase in the critical Reynolds number from $Re_{C_1} = 46$ for $G/D \to \infty$ to $Re_{C_1} > 100$, for gaps below $G/D \lesssim 0.4$.

More recently, Rao et al. (2013, 2015b) simulated the flow past nonrotating and rotating circular cylinders moving through a fluid at different heights above a no-slip plane boundary for $Re \leq 400$. The series of 2D vorticity fields in **Figure 6** shows in more detail the changes to the flow physics caused by wall proximity. As the gap gets smaller, the increasing blockage reduces the circulation fed into the lower vortices shedding into the wake, affecting the symmetry between positive and negative vortices forming the vortex street. In addition, for small gaps, the proximity of the upper shed vortices to the wall induces opposite-signed secondary vorticity there that can be advected into the wake to pair with the primary vortices. Thus, the character of the wake changes as the gap is reduced, and with it the nature of the first transition from steady 2D flow. Whereas this transition occurs through a Hopf bifurcation to periodic flow at large gaps, a regular bifurcation leads to steady 3D flow (mode E) for small gaps. Similarly, the onset of the 3D mode A instability, and indeed whether it is the first 3D instability, is very sensitive to gap size.

**Figure 7** summarizes the various transitions and unstable wake modes for cylinders moving along a wall, as function of Reynolds number and gap size, and also for the cases with simultaneous forward or backward rotation. Gap size has a strong influence in the range $G/D \lesssim 0.4$; for higher values, the transition sequence is close to that of an isolated cylinder. Some of the 3D instability modes are depicted in **Figure 8**. As for the isolated cylinder, they include a subharmonic mode (mode C′), as well as a steady 3D mode (E) at different spanwise wavelengths.

## 3.2. Spheres

Among studies conducted on rotating spheres near boundaries are the works of Zeng et al. (2005) and Cherukat & McLaughlin (1994), the latter being restricted to the Stokes regime, where a sphere is moving parallel to a wall at a distance of 0.25 sphere diameters or greater and is free to rotate. Their results indicate that, in general, any observed induced rotation is in the prograde rotation direction and that this rotation has little effect on the lift and drag forces. The transition to unsteady flow with hairpin vortices and loops in the wake occurs earlier than for an isolated sphere, with the critical Reynolds number decreasing as the distance to the wall is reduced. At the lowest gap ratio tested ($G/D = 0.25$), a sudden increase was observed: The wake remained steady beyond

**Prograde rotation:** rotation in the same direction as for rolling without slip

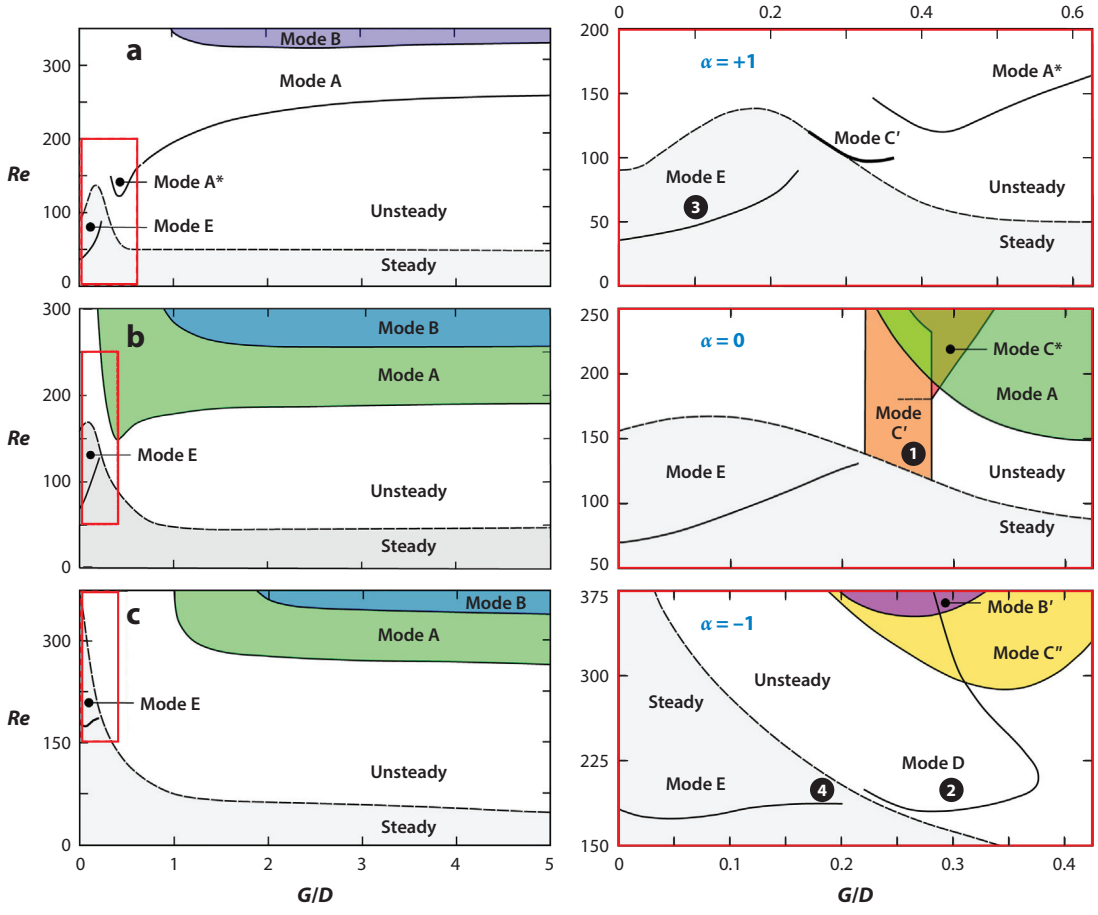


**Figure 7**

Parameter space showing the wake modes of a cylinder of diameter $D$ translating near a wall with gap $G$ for (*a*) forward (normal) rotation ($\alpha = +1$), (*b*) no rotation ($\alpha = 0$), and (*c*) backward (reverse) rotation ($\alpha = -1$). The transition from steady to unsteady flow is marked by a dashed line. Diagrams on the right are enlargements of the regions outlined in red on the left. Circled numbers refer to the modes shown in **Figure 8**. Figure adapted with permission from Rao et al. (2015b), copyright 2015 Elsevier.

$Re = 300$. Zeng et al. (2005) related this behavior to the competition between asymmetry (promoting early shedding) and viscous effects (delaying the transition), both induced by the presence of the wall.

**Lubrication theory:** modeling of the flow in a thin fluid layer bounded by solid surfaces, neglecting inertial effects

The behavior of the lift and drag coefficients of spheres translating close to a wall was investigated by Zeng et al. (2009) at moderate Reynolds numbers covering the steady regimes ($Re < 300$). Force coefficients for spheres are defined in the standard way through $F = C_F \cdot \frac{1}{2}\rho U^2 \cdot \frac{\pi}{4}D^2$, where $F$ is the corresponding force and $\rho$ the fluid density. These force coefficients, as a function of Reynolds number and gap ratio, are summarized in **Figure 9** for the case of pure translation, as predicted by Zeng et al. (2009) and others. The isolated sphere drag variation, together with predictions of lubrication theory, is also provided for comparison. Orders-of-magnitude changes in both the drag and lift coefficients are observed as the Reynolds number and gap ratio are varied, the latter showing the profound effect of the wall. Note that the lift remains finite for all parameter

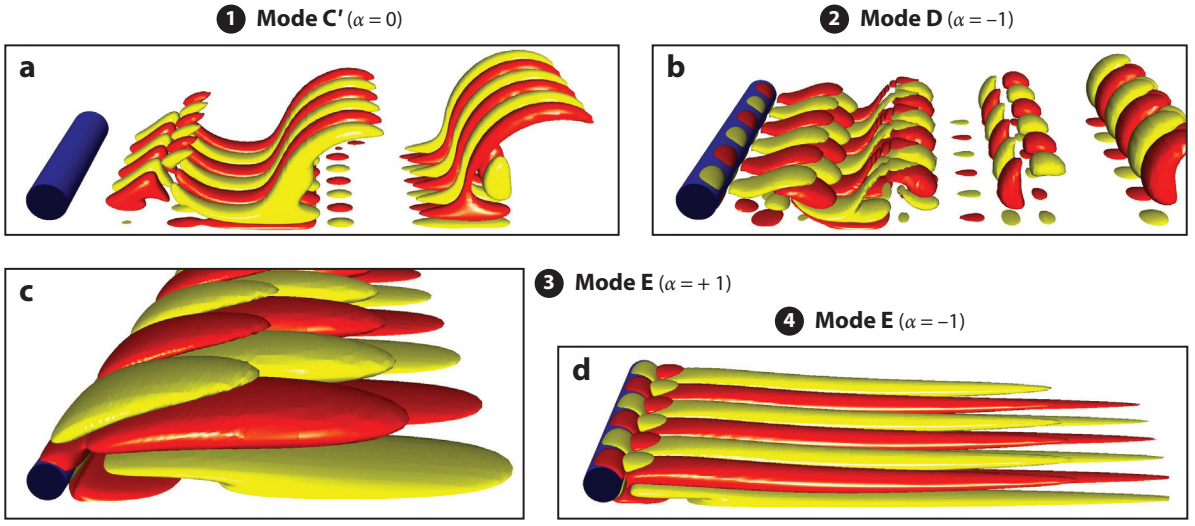


**Figure 8**

Three-dimensional instability modes of the wake of a cylinder of diameter $D$ translating parallel to a wall, visualized by isosurfaces of positive and negative streamwise vorticity. (*a*) Subharmonic mode C′ with a spanwise wavelength $\lambda/D = 1.35$ for the sliding cylinder ($\alpha = 0$). (*b*) Periodic mode D with $\lambda/D = 2.6$ for the cylinder in reverse rotation ($\alpha = -1$). (*c*) Steady mode E with $\lambda/D = 11$ for the cylinder in normal rotation ($\alpha = +1$). (*d*) Steady mode E with $\lambda/D = 2.75$ for the cylinder in reverse rotation ($\alpha = -1$). Circled numbers refer to the locations in the parameter space shown in **Figure 7**. Figure adapted with permission from Rao et al. (2015b), copyright 2015 Elsevier.

values, whereas the drag diverges logarithmically and as $Re^{-1}$ for vanishing gap size and Reynolds number, respectively.

## 4. BLUFF BODIES ROLLING ALONG A WALL

### 4.1. Rolling Circular Cylinders

As discussed in Section 3.1, the immediate proximity of a wall suppresses the passage of fluid underneath the cylinder, leading to single-sided vortex shedding into the wake. In turn, the proximity to the wall of these shed vortices induces secondary wall vorticity, which separates and rolls up into weaker vortex structures that pair with the primary vortices to form the wake. The addition of prograde (normal) rolling to the scenario has two main effects: It increases the circulation fed into the upper primary vortices (because of the increased velocity gradient at the cylinder surface), and it also leads to separation at a smaller angle from the front of the cylinder, so that these vortices advect into the wake further away from the wall. These two effects affect the magnitude of the secondary wall vorticity generated and so influence the structure and stability of the wake. The details were explored experimentally and numerically by Stewart et al. (2006, 2010b) for cylinders moving at constant speed with a very small fixed gap ($G/D = 0.005$) and for $Re \leq 350$. The transition map as a function of Reynolds number and rotation rate is given in **Figure 10*a***. For a nonrotating (sliding) cylinder, the 2D flow remains steady up to $Re = 165$, beyond which periodic flow is observed, where opposite-signed vortex structures combine and self-propel away from the wall. Linear stability analysis was used to show that the flow becomes 3D directly from steady flow at $Re = 70.5$. This is unlike the situation for an isolated cylinder, where transition to 3D flow occurs from a periodic wake. The transition Reynolds numbers vary with the rotation

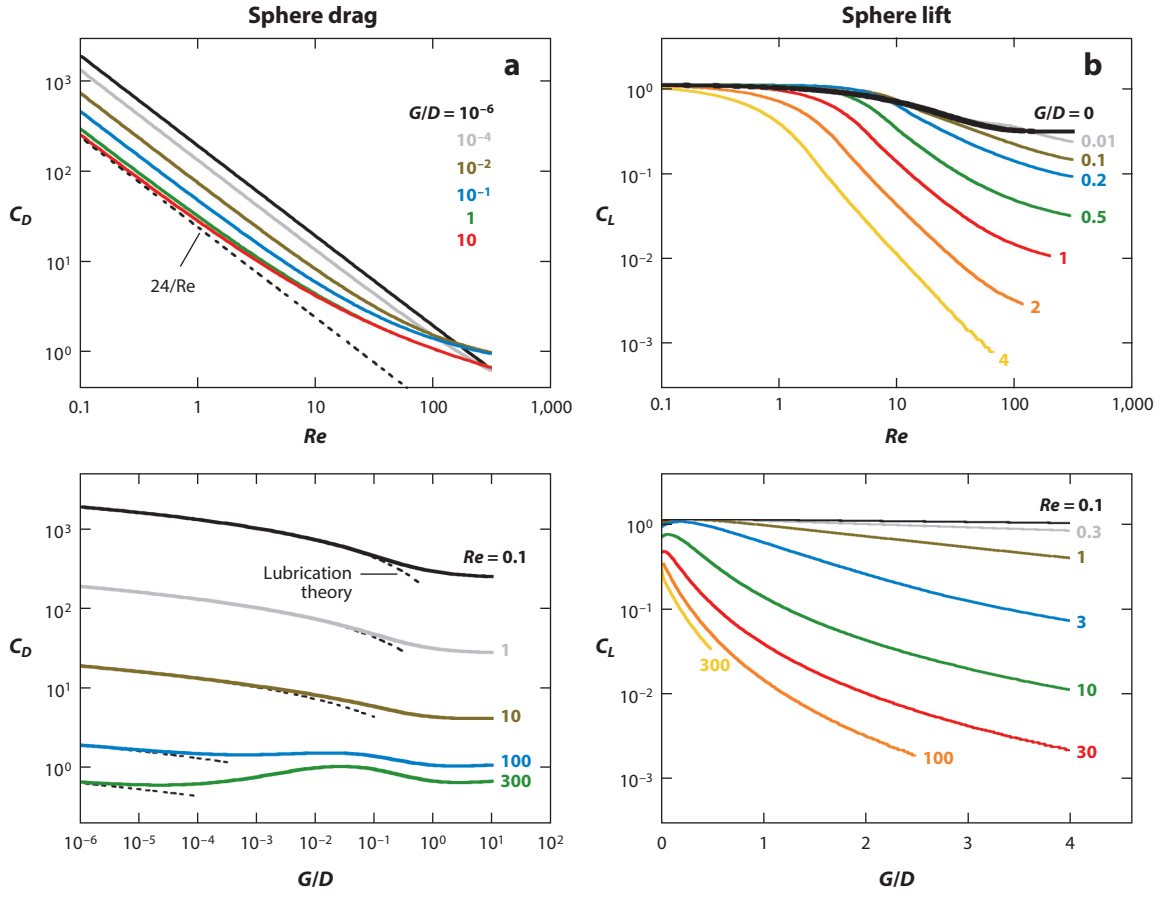


**Figure 9**

(*a*) Drag coefficient $C_D$ and (*b*) lift coefficient $C_L$ for a nonrotating sphere of diameter $D$ moving parallel to a solid wall in a quiescent fluid, as a function of Reynolds number $Re$ (*top*) and of gap size $G$ (*bottom*). The limits for Stokes flow at large gaps and for lubrication at vanishing gaps (Goldman et al. 1967) are shown as dashed lines. Diagrams were computed using the correlations proposed by Zeng et al. (2009) based on a survey of various experimental and numerical studies.

rate and increase with decreasing $\alpha$, and vice versa. Water-tunnel wake visualizations are in good agreement with the numerical simulation predictions, as can be seen, e.g., for the forward- and reverse-rolling cases shown in **Figure 11**. More recently, Houdroge et al. (2017) examined the onset of three-dimensionality of a cylinder rolling freely along a wall without slip ($\alpha = 1$), again through experiments and numerical simulation. **Figure 12** shows that three-dimensionality can strongly distort the wake structures after a few shedding cycles at moderate Reynolds numbers, and additionally that the influence of the free ends of the cylinder propagates rapidly inward along the span.

## 4.2. Rolling Spheres

While maintaining some of the flow physics governing rolling-cylinder wakes, there are also some important differences for rolling spheres. In particular, a rolling sphere touches the surface at a single point rather than along a line, which allows the fluid to pass around the sides of the sphere

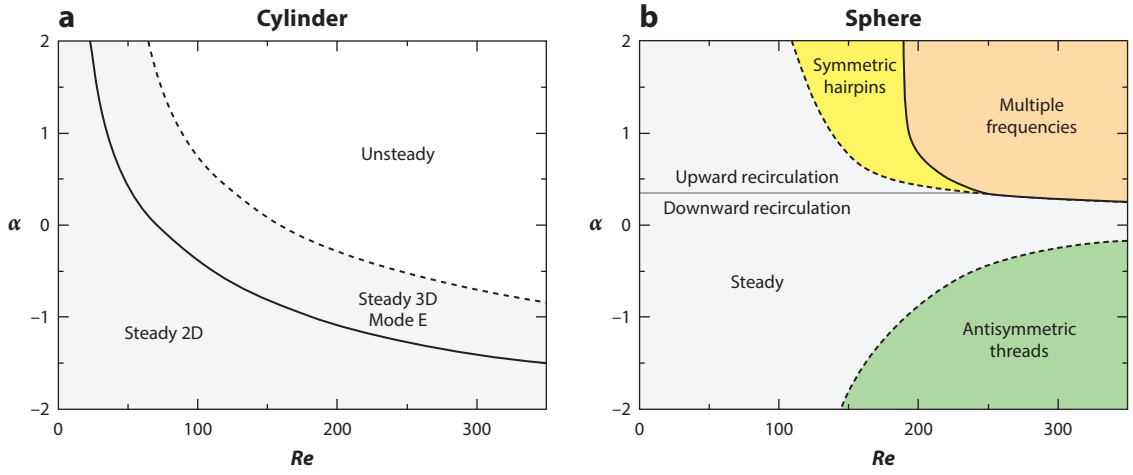


**Figure 10**

Wake regimes for (*a*) a cylinder and (*b*) a sphere of diameter $D$ translating along a wall and rotating at different rates, $\alpha$. The gap size is $G/D = 0.005$. Diagrams based on results from numerical simulations and stability analyses by Stewart et al. (2010a,b) and Rao et al. (2011, 2012).

as the gap is reduced. For this reason, wall proximity has a reduced influence in modifying the wake from that of the isolated sphere, compared to the cylinder case. This problem has been explored by Stewart et al. (2008, 2010a) and Rao et al. (2012) for the flow around spheres translating at constant speed and rotating very close to a wall at Reynolds numbers up to several hundred, covering both steady and unsteady regimes. The gap ratio was chosen to be sufficiently small ($G/D = 0.005$), so that the wake flow structures are not sensitive to the gap, even though the lift and drag forces are, as discussed below in Section 4.3. The effect of the sign and magnitude of the rotation rate on the wake characteristics up to $Re = 350$ is shown in **Figure 10*b***.

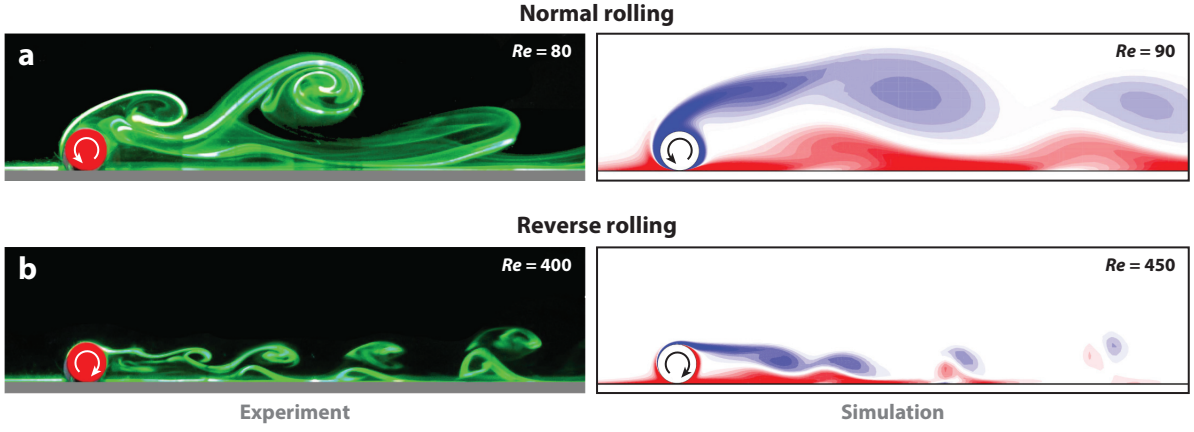


**Figure 11**

Unsteady two-dimensional wake of a cylinder translating on a wall, for (*a*) normal rolling ($\alpha = +1$) and (*b*) reverse rolling ($\alpha = -1$): (*left*) experimental dye visualizations in a water channel equipped with a moving floor; (*right*) vorticity fields from numerical simulation. Figure adapted with permission from Stewart (2008).

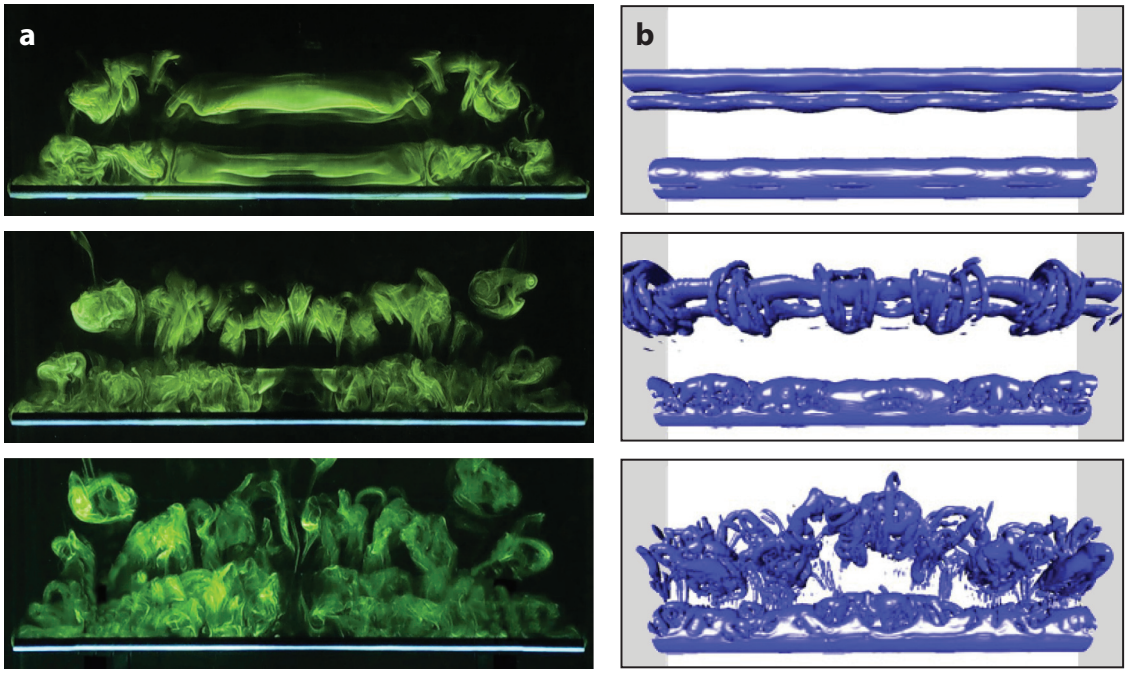


**Figure 12**

Development of three-dimensionality in the wake of a freely rolling cylinder of diameter $D$ at $Re = 160$. (*a*) Experimental dye visualization of the first three shedding cycles after an impulsive start from rest. The cylinder is $47D$ long, with free ends. (*b*) Isosurface of the $Q$-criterion function (Hunt et al. 1988) from numerical simulation, showing vortical structures during three consecutive shedding cycles after the onset of three-dimensional flow. The cylinder length is $54D$, with periodic boundary conditions. Panel *b* adapted with permission from Houdroge et al. (2017), copyright 2017 Cambridge University Press.

For $\alpha > 0$ (prograde rolling), a compact zone of recirculating fluid is formed and the unsteady flow is marked by the shedding of hairpin vortices analogous to the periodic wake of an isolated sphere. However, for $\alpha < 0$ (retrograde rolling), a streamwise vortex pair appears in the wake, and as $Re$ is increased further the wake undergoes a transition to an antisymmetric mode. A comparison between these two wake states is given in **Figure 13**.

For the forward-rolling sphere with $\alpha = 1$, the wake remains attached and steady at low Reynolds numbers (Stewart et al. 2010a); it is analogous to that of an isolated sphere, i.e., a double-threaded wake consisting of a counter-rotating vortex pair. Transition to unsteady, periodic, and symmetric flow occurs at $Re \simeq 139$, as shown through direct numerical simulations by Rao et al. (2012), who also identified a second transition at $Re \simeq 192$ to unsteady, asymmetrical flow, where the wake exhibits oscillations in the lateral directions. Both transitions were found to be supercritical (nonhysteretic). Visualizations of the symmetric and asymmetric unsteady wakes are shown in **Figure 14**.

**Vortex-induced vibrations:** body oscillations caused by time-dependent fluid forces due to vortex shedding

In general, when a body is not forced to move at a constant speed, e.g., in cases where it is rolling down a slope driven by gravity, unsteadiness in its wake leads to oscillations (vibrations) of its trajectory. As well as sphere oscillations in the downslope direction, there is also considerable movement across the slope. The sidebar titled Vortex-Induced Vibrations of Rolling Bodies gives a few brief details concerning this topic, which is beyond the scope of the present review.

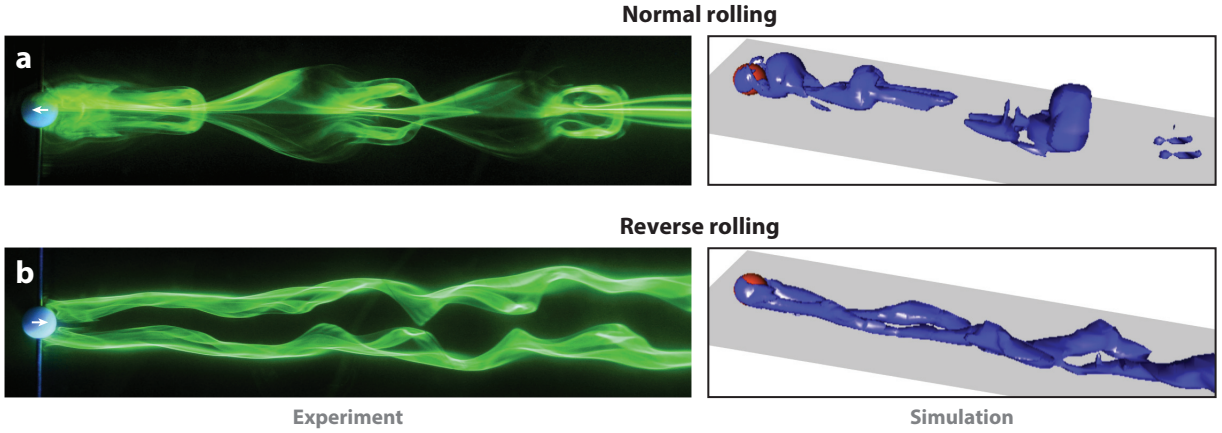


**Figure 13**

Unsteady wake of a sphere translating on a wall, for (*a*) normal rolling ($\alpha = +1$) and (*b*) reverse rolling ($\alpha = -1$). (*Left*) Experimental dye visualizations (top view) at $Re = 200$ in a water channel equipped with a moving floor. Visualizations reprinted with permission from Stewart et al. (2008), copyright 2008 AIP Publishing. (*Right*) Vortical structures (oblique view) from numerical simulation, visualized by the method proposed by Jeong & Hussain (1995), at $Re = 200$ (*top*) and $Re = 300$ (*bottom*). Simulation results adapted with permission from Stewart et al. (2010a), copyright 2010 Cambridge University Press.

Theoretical analysis has been combined with laboratory experiments to investigate the forces acting on a sphere rolling freely down an incline (Carty 1957, Garde & Sethuraman 1969, Jan & Shen 1995, Verekar & Arakeri 2010). The sphere eventually reaches a terminal velocity from which an effective drag coefficient ($C'_D$) can be calculated. Note that for a sphere rolling down a slope without slip, this effective $C'_D$ is given by the sum of the standard drag coefficient and the fluid torque coefficient. The data are presented in the composite plot of **Figure 15*a***. They

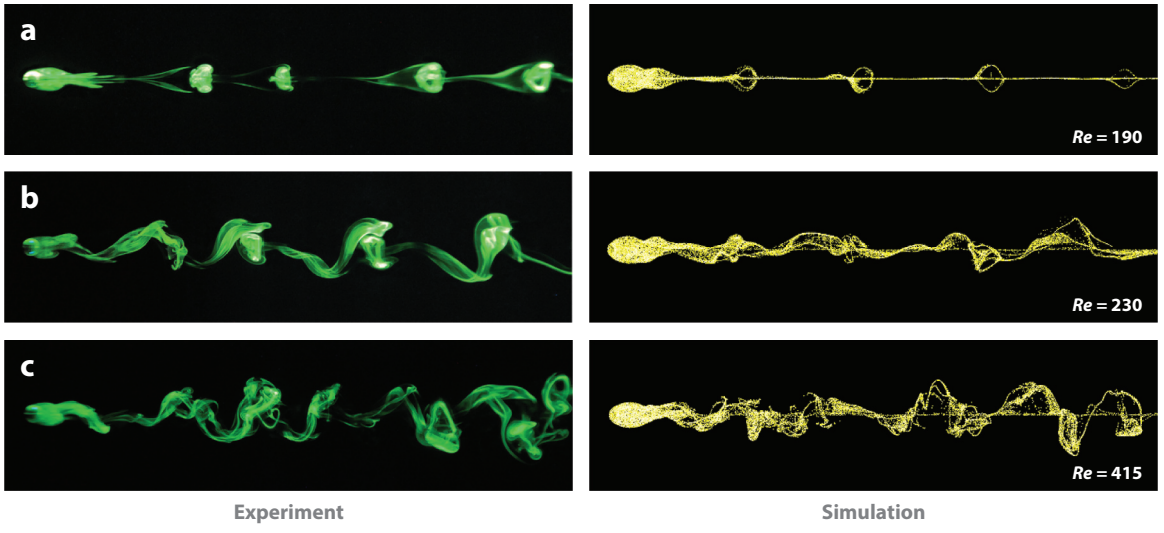


**Figure 14**

Wake of a sphere rolling in a straight line along a wall at $Re = 190$ (*a*), $Re = 230$ (*b*), and $Re = 415$ (*c*), seen from above: experimental dye visualization (*left*) and numerical simulation with tracer particles (*right*). A bifurcation breaking the initial planar symmetry occurs at $Re = 192$, between panels *a* and *b*. Figure adapted with permission from Rao et al. (2012), copyright 2012 Cambridge University Press.

## VORTEX-INDUCED VIBRATIONS OF ROLLING BODIES

Vortex-induced vibration (VIV) of rotating bodies is also influenced by the presence of a wall compared to isolated cases (Bourguet & Lo Jacono 2014, Zhao et al. 2018), along with changes to the potential added mass. For a body accelerating in a fluid, the fluid force (drag) resisting this acceleration can be expressed as a mass that is added to the body mass in the equations for the body motion. The added mass coefficient is the ratio of this additional mass to the fluid mass displaced by the body. For a cylinder and a sphere, this coefficient increases from 1 and 1/2, respectively, at infinity, to approximately 2.29 and 0.58, respectively, at the wall for motion parallel to the wall, independent of rotation (Brennen 1982). These increases represent an added resistance to acceleration of the bodies, which should act to mitigate VIV to some extent. However, there are also dramatic changes in the wake structures, for both rolling cylinders (Houdroge et al. 2020) and rolling spheres (F.Y. Houdroge, J. Zhao, T. Leweke, K. Hourigan & M.C. Thompson, submitted manuscript), at least in the low–Reynolds number range. These bodies are found to undergo increasing VIV about their mean rolling speed with decreasing ratio of body and fluid densities; interestingly, spheres have considerably smaller vibration amplitudes than cylinders.

show that, for low Reynolds numbers, the drag is significantly greater than for a sphere in an unbounded flow (compare with **Figure 9*a***), but it also appears to vary as $Re^{-1}$ up to $Re \approx 100$. Although Carty (1957) and Garde & Sethuraman (1969) followed a similar experimental methodology, drag coefficients calculated in the latter study are up to twice as large as those from the former. Garde & Sethuraman (1969) related this difference to the longer experimental flume used in their experiments, which led to more accurate timing and therefore velocity calculations, although their graph has a significant amount of scatter. For $Re \geq 5$, the results of Jan & Shen (1995) are broadly consistent with, although generally well above, the observations of Carty (1957), and their

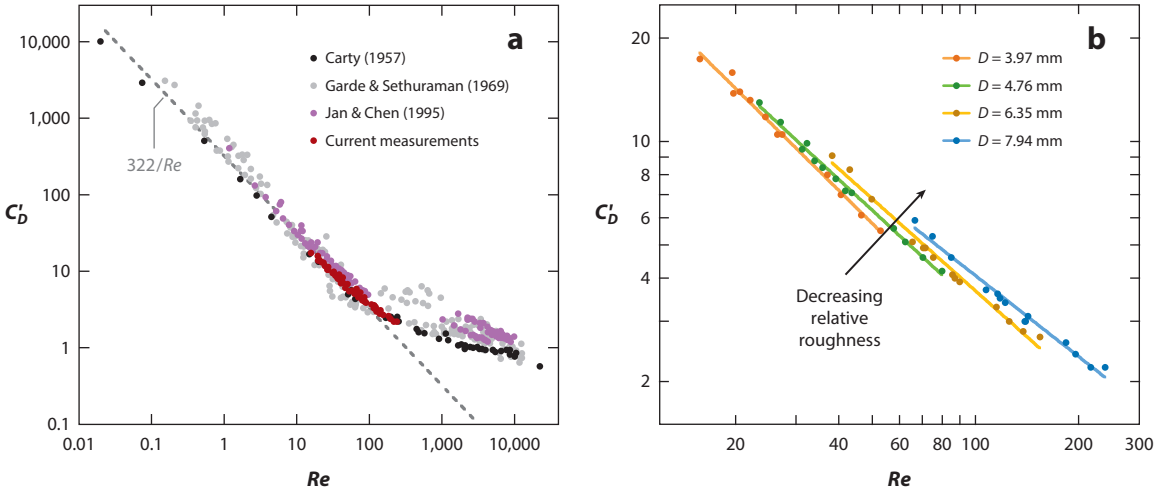


**Figure 15**

Mean effective drag coefficient $C'_D$ (including torque) of a sphere rolling down an incline, as function of Reynolds number $Re$. (*a*) Collection of various experimental data. (*b*) Close-up of the current measurements (F.Y. Houdroge, J. Zhao, T. Leweke, K. Hourigan & M.C. Thompson, submitted manuscript), showing an increase of the drag with decreasing relative surface roughness (increasing diameter) of the sphere.

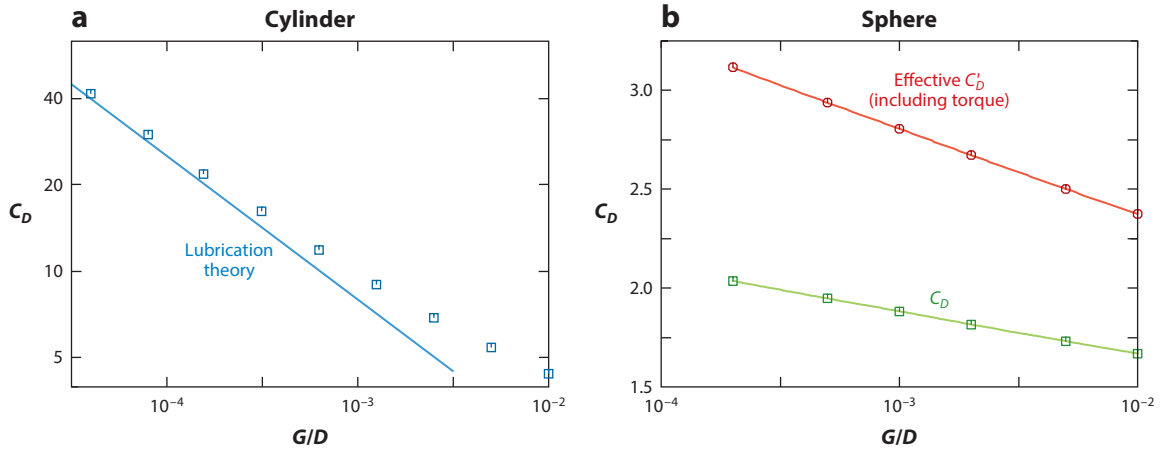


**Figure 16**

Drag coefficient $C_D$ for rolling bodies of diameter $D$ as function of gap size $G$ from direct numerical simulation. (*a*) Cylinder at $Re = 50$. The line shows the prediction from lubrication theory: $C_D = 4\pi/[Re(G/D)^{1/2}]$. Panel *a* adapted with permission from Houdroge et al. (2020). (*b*) Sphere at $Re = 100$. The lines represent scalings in line with lubrication theory: $C_D \sim [\ln(D/G) + \text{const.}]$.

data show considerable scatter, too. It is also unclear why they do not present any values in the $100 < Re < 1{,}000$ range.

## 4.3. The Rolling Paradox

Many careful experimental and numerical studies have been undertaken concerning the dynamics of rolling/sliding cylinders and spheres in close proximity to a wall. For the numerical studies, in particular, a finite gap has been maintained between the cylinder and the wall due to the problem of a mesh singularity arising at zero gap, and also to keep a reasonable computational time step, since the respective timescales governing the gap flow and the global wake dynamics become increasingly separated. For small gaps ($G/D \lesssim 0.01$), vortex formation and shedding is relatively independent of the gap size, but the force coefficients are strongly affected, as shown by the examples in **Figure 16** (see also **Figure 9**). The so-called rolling paradox arises from theoretical/analytical results concerning the flow in the gap region using lubrication theory. This theory was applied to the rolling cylinder and rolling sphere problems by, e.g., Merlen & Frankiewicz (2011) and Goldman et al. (1967), respectively. They predicted that, as the gap size approaches zero, the drag force on the body diverges as $(D/G)^{1/2}$ for the cylinder and as $\ln(D/G)$ for the sphere, for any combination of sliding and rolling, due to the generation of a pressure peak diverging to positive infinity in front of the body, and another peak diverging to negative infinity behind it. This implies that a cylinder or sphere in contact with a solid surface would be impossible to move along this surface, which is contrary to common observation, and that any rolling or sliding motion along the wall would involve a liquid film of finite thickness between the two, i.e., the absence of solid-to-solid contact. Goldman et al. (1967) calculated that the gap size compatible with the drag coefficients of a rolling sphere determined experimentally by Carty (1957) (**Figure 15*a***) would be of the order of atomic dimensions, which is well outside the validity domain of the theory. Goldman et al. (1967) put forth six points of discussion in an attempt to explain the discrepancy between the idealized model provided by lubrication theory and experimental data. They include the roughness of the sphere or wall, compressibility effects and cavitation linked to the large

negative pressures encountered, breakdown of the continuity assumption at very small gaps, inertial and non-Newtonian effects, and deformations of the sphere by the high pressure gradient.

Surface roughness was dismissed by Goldman et al. (1967), since Carty's (1957) drag data apparently did not show differences between the various spheres of different roughnesses used. It appears that this conclusion is not clearly justified by the data (**Figure 15**). Specifically, the data points are not frequent enough to allow for differentiation, and the results are presented on a log–log plot that masks any such trends. (On such a log–log plot with sparse points, a variation in drag coefficient of 100% is essentially not discernible!) More recent experiments appear to show that different relative surface roughnesses do in fact lead to different drag coefficient variations with macroscopic Reynolds number, as seen in **Figure 15*b***. By providing an effective average gap, the roughness of the body (or wall) appears to be a determining factor for its motion along a wall. Interestingly, the drag prediction from direct numerical simulation for smooth rolling spheres at higher Reynolds number (**Figure 16*b***) appears to approach the experimentally observed values given by Carty (1957) (**Figure 15**), as the gap ratio approaches expected relative roughness ratios ($\delta/D \sim 10^{-6}$–$10^{-7}$, where $\delta$ is the mean asperity height).

Roughness effects were further investigated by Smart et al. (1993), who extended the work of Goldman et al. (1967) by proposing that roughness elements can in fact lead to physical contact with the plane when the separation distance between the surfaces is of the order of the roughness height, and that the plane will then exert a nonhydrodynamic force and torque on the sphere. Their research gave quantitative agreement between measured translational and rotational velocities and their theory for small inclination angles of the plane; however, their data at high angles showed a greater discrepancy, in line with a larger apparent gap than the one considered. King & Leighton (1997), Galvin et al. (2001), and Zhao et al. (2002) argued that rather than experiencing a single surface roughness and separation distance, the sphere has two scales of roughness: small bumps that support the particle at rest and at low angles, and larger roughness elements distributed sparsely on the surface that dominate the separation at higher angles. Galvin et al. (2001) and Zhao et al. (2002) developed a theoretical model of this phenomenon and tested it experimentally, confirming that, at low angles, the sphere is in contact with the wall via the small asperities, whereas at high angles the large asperities may cause the sphere to lift off the wall and move without continuous contact.

Although a smooth bump, no matter the radius, will induce an unlimited pressure force as the gap between it and a smooth surface decreases, a roughness element or asperity of small enough dimension can decrease the gap to molecular dimension, whereby contact can be said to occur (Smart & Leighton 1989, Lecoq et al. 2004). The observation that in practice contact does occur is therefore a consequence of physical considerations outside the assumptions of surface smoothness, fluid continuum, and incompressibility, such as roughness closing the gap to the order of the fluid molecular dimension, or ultimately other short-range interactions like van der Waals forces. The precise details of how solid-to-solid contact occurs, which are essential for an understanding of the resistive forces due to contact, the effective hydrodynamic gap, and the rolling speed of bluff bodies, are presently still not entirely clear.

When the body is surrounded by a liquid, cavitation can occur for small gaps, when the diverging negative pressure decreases below the vapor pressure, an effect already investigated by Taylor (1963) for lubrication flow. Merlen & Frankiewicz (2011) and Prokunin (2003) have analyzed the cases of cylinders and spheres rolling along a plane wall. When cavitation appears, it eliminates the large negative pressure peak behind the body, but not the positive peak ahead of it. This asymmetry results in a net lift force that can push the body further away from the surface, while at the same time maintaining a large drag force. (Similarly, fluid compressibility modifies the pressure distribution near contact but infinite pressures still arise from zero gap.) Experiments by Seddon

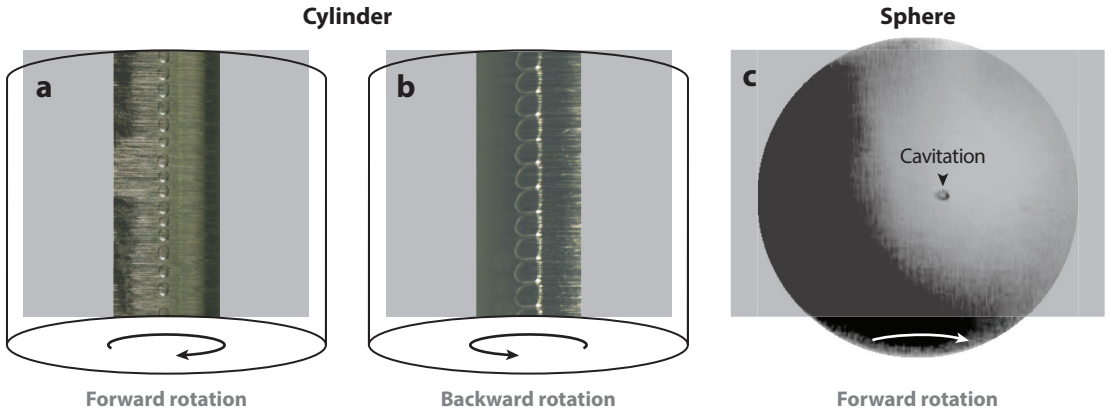


**Figure 17**

Experimental visualization of cavitation bubbles in the gap region of bluff bodies moving along a wall in Stokes flow. Views from below through the transparent wall. All bodies move to the left. (*a*) Cylinder in forward rotation ($Re = 1.2$, $\alpha \approx 1$). (*b*) Cylinder in backward rotation ($Re = 2.9$, $\alpha \approx -0.2$). Panels *a* and *b* adapted with permission from Seddon & Mullin (2006), copyright 2006 AIP Publishing. (*c*) Sphere in forward rotation ($Re = 0.5$, $\alpha \approx 0.3$). Panel *c* adapted with permission from Ashmore et al. (2005), copyright 2005 American Physical Society.

& Mullin (2006) on cylinders moving close to a wall in a highly viscous liquid have shown that cavitation appears in the gap region in the form of a periodic array of vapor bubbles (**Figure 17*a***), whereas Prokunin (2004) and Ashmore et al. (2005) visualized a single cavitation bubble for the case of a rolling sphere (**Figure 17*b***).

## 5. BLUFF BODIES IMPACTING ON A WALL

In this section, we are chiefly concerned with the flow structures arising from a rigid body impacting on a rigid wall, and not the elastic or plastic deformations that may occur in the solid structures (for the latter, see, e.g., Yildirim et al. 2017). In this case, the initial stage of the wake evolution is clearly related to those of impulsively arrested bodies discussed in Section 2.3. In addition, in a broader sense, the later wake evolution involves secondary vorticity generation from the proximity of primary vortices to the wall, which subsequently leads to vortex pair formation and self-propulsion away from the body, showing similarities with the wake evolution of rolling or sliding bodies discussed in Section 4.

### 5.1. Impacting Cylinders

Leweke et al. (2008) presented results from experiments and simulations on the flow around a circular cylinder upon impact with a solid wall. At low Reynolds numbers, when impacting normally to the wall, the attached counter-rotating vortices that form during the pre-impact motion of the cylinder overtake it on impact, one on each side, and then initially move outward along the wall due to the influence of their image vortices. Subsequently, the vortices experience a weak rebound associated with secondary vorticity generated at both the cylinder and wall (**Figure 18*a***). For higher Reynolds numbers, the secondary vorticity generated rolls up into discrete secondary vortices that orbit the primary vortices and undergo a 3D elliptic instability (**Figure 19*a***), a phenomenon known to occur in strained vortical flows (Kerswell 2002). Beyond a Reynolds number of a few hundred, this process leads to breakdown of the vortex system into small-scale structures.

**Image vortices:** virtual vortices located symmetrically with respect to a surface, having the same effect as the boundary condition of zero normal velocity at this surface

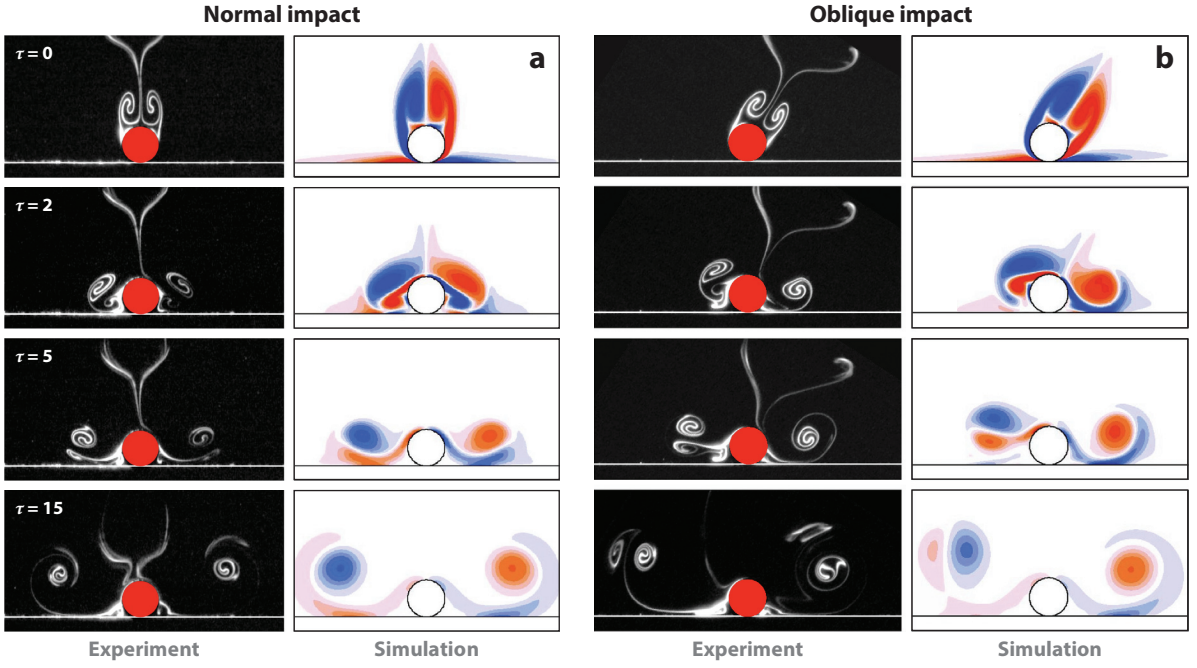


**Figure 18**

Flow generated by a circular cylinder of diameter $D$ translating a distance $L$ before impacting on a solid wall at $Re = 200$, with $L/D = 4$. Experimental dye visualization and numerical vorticity fields. (*a*) Normal impact, and (*b*) oblique impact at $\theta = 57°$. Nondimensional time $\tau = tU/D$ is counted from the moment of impact. Figure adapted with permission from Leweke et al. (2008), copyright 2008 Elsevier.

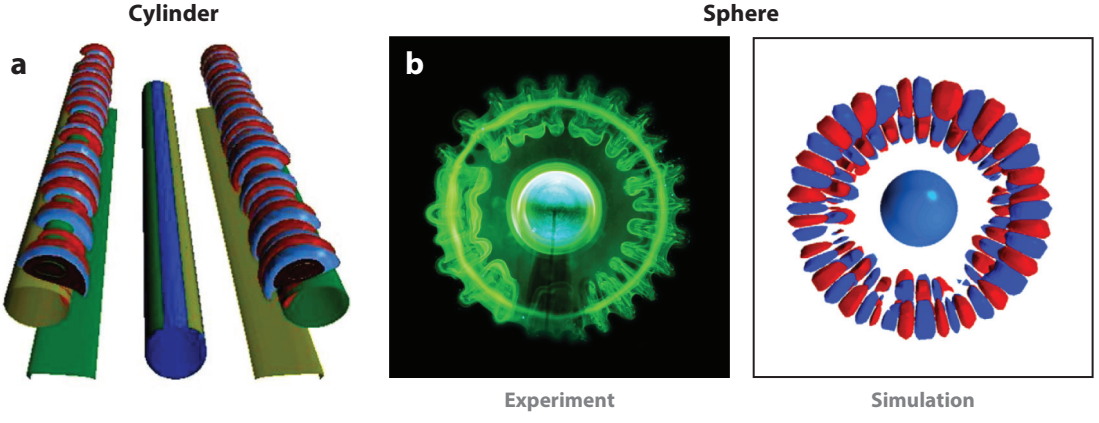


**Figure 19**

Three-dimensional instability of the flow generated by the impact of a body of diameter $D$ on a wall after translating a distance $L$. (*a*) Cylinder at $Re = 400$ for $L/D = 5$. Isosurfaces of vorticity from numerical simulation, showing an elliptic instability of the secondary vortex. Panel *a* adapted with permission from Thompson et al. (2006a), copyright 2006 Elsevier. (*b*) Sphere for $L/D = 5$. Dye visualization in water at $Re = 1{,}500$ (*left*) and isocontours of radial vorticity from simulation at $Re = 1{,}200$ (*right*), showing the centrifugal instability of the primary vortex. Panel *b* reprinted with permission from Leweke et al. (2004b), copyright 2004 AIP Publishing.

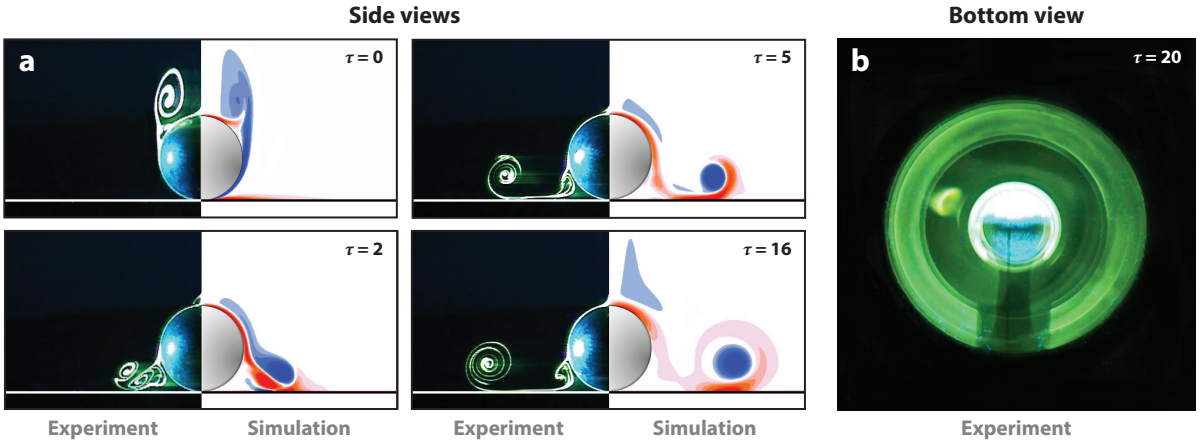


**Figure 20**

Wall impact of a sphere of diameter $D$ after translating a distance $L$ at $Re = 800$, with $L/D = 5$. (*a*) Side views with experimental dye visualizations and numerical vorticity fields. Panel *a* adapted with permission from Leweke et al. (2004b), copyright 2004 AIP Publishing. (*b*) Bottom view: experimental dye visualization. Panel *b* reprinted with permission from Leweke et al. (2004a), copyright 2004 AIP Publishing.

This flow behavior is similar to the case of a counter-rotating vortex pair impinging on a solid wall (Leweke et al. 2016).

Oblique cylinder impacts have also been examined (**Figure 18*b***). Not surprisingly, this asymmetry leads to different flows generated on each side of the cylinder. The vortical structures that develop on the side beneath the cylinder path appear similar to those for the normal impact case, while generation of secondary vorticity at the wall on the opposite side decreases with growing impact angle, leading to changes in the pair formation process. For higher-impact angles, the source of secondary vorticity generation is mostly restricted to the cylinder surface, resulting in the formation of a vortex dipole that, through self-induction, leads to rebound and self-advection of the primary vortex to greater heights than occurs for the normal impact.

## 5.2. Impacting Spheres

The flow generated by the normal impact of a sphere on a wall bears similarities with the cylinder case. The recirculation zone behind the moving sphere here takes the form of a vortex ring. On impact, this ring overtakes the sphere, leading again to the generation of secondary vorticity at the sphere surface and at the wall, which separates and wraps around the primary ring (**Figure 20**). At low Reynolds numbers, the flow remains axisymmetric at all times, whereas for $Re \gtrsim 1{,}000$, an instability develops in the azimuthal direction of the primary vortex ring, as seen in **Figure 19*b***. Leweke et al. (2006) endeavored to gain an understanding of the flow physics involved in this instability. They found that the flow structures that developed were consistent with a centrifugal instability of the primary vortex ring core surrounded by secondary vorticity of opposite sign drawn up from the wall. Both the growth rate and azimuthal mode numbers, predicted from idealized centrifugal instability theory based on the local velocity profile, show good agreement with those observed in the experiments, simulations, and linear stability analysis of the frozen flow state. Since the cross section of the primary ring becomes elliptical after the impact, the stability of the ring was also tested against elliptic instability. Although the predicted azimuthal mode numbers matched well, the predicted growth rates were negative.

The dynamics bears resemblance to the related case of a vortex ring impacting on a wall, studied by Walker et al. (1987), Lim (1989), Lim et al. (1991), Orlandi & Verzicco (1993), Swearingen et al. (2000), and Masuda et al. (2012). In both configurations, the primary vortex ring draws up secondary vorticity generated as it nears the wall, and then the ring structure expands radially, leading to qualitatively similar vorticity patterns. However, the isolated impacting ring becomes unstable through fragmentation of the secondary vorticity into quasi-discrete vortices when the Reynolds number is sufficiently large. This secondary vortex fragmentation has a relatively low azimuthal wavenumber (∼6 waves along the ring perimeter, compared to ∼20 for the sphere impact in **Figure 19*b***) and involves self- and mutual induction from the primary vortex, as discussed in the above articles. Of interest, direct simulations of vortex ring impact have indicated that this fragmentation process arrests relatively quickly, and subsequently a shorter-wavelength instability manifests, possibly attributable to the same centrifugal mechanism causing ring breakup for the sphere impact.

Comparisons between circular cylinder impact and normal sphere impact have revealed important differences in the developed wakes. The vortex stretching of the primary vortex as the ring expands radially is not present for the cylinder impact, and this leads to a reduction in core size and accelerated vorticity cross-diffusion in the axisymmetric geometry. These effects delay the onset of 3D instabilities in the vortical flows generated upon impact of a spherical particle with a wall, in comparison to the 2D counterpart.

In comparison with the flow generated by a body arrested in isolation (Section 2.3), the presence of the wall has two main effects: It restricts and modifies the trajectories of the primary vortices, through induction from the image vortices representing the boundary condition of vanishing normal flow velocity at the wall, and it is a further source of secondary vorticity. Together, these effects can produce vortex configurations not found for freely arresting bodies, e.g., where the secondary vorticity wraps around the primary vortex in a band (**Figures 18*a*** and **20*a***) instead of forming a discrete concentrated vortex (**Figure 5**), which can lead to different types of 3D instability (centrifugal instability) at higher Reynolds numbers.

## 5.3. Rebounding Bluff Bodies

The configuration involving a spherical particle in a viscous fluid rebounding from a solid surface after a normal collision has been investigated in numerous studies including analytical/numerical work by Davis et al. (1986), Lian et al. (1996), Ardekani & Rangel (2008), Li et al. (2012), and Brändle de Motta et al. (2013), as well as in experiments by Gondret et al. (1999, 2002), Joseph et al. (2001), and Ruiz-Angulo & Hunt (2010). Most of these studies focused on the flow structure around the point and near the time of impact, and on the determination of the coefficient of restitution ($\varepsilon$), given by the ratio of rebound velocity to particle impact velocity. Few studies have considered the vortical structures in a more extended region and time interval around the collision. The visualization by Thompson et al. (2007) and simulations by Ardekani & Rangel (2008) show that the primary vortex ring in the wake of the approaching sphere is left behind after the rebound and exhibits dynamics similar to that for a sphere with no rebound (compare **Figures 20** and **21*a*,*b***).

The coefficient of restitution was found to depend on the nondimensional Stokes number, $Stk = (1/9)(\rho_p/\rho_f)Re$, where $\rho_p$ and $\rho_f$ are the particle and fluid densities, respectively, and $Re$ is the particle Reynolds number at impact, with only a weak dependence on the elastic properties of the material (Joseph et al. 2001). This parameter compares particle inertia to viscous effects; according to Legendre et al. (2005), the effect of added mass should also be included: $Stk^* = (1/9)(\rho_p/\rho_f + C_m)Re$, with $C_m$ the added mass coefficient. No rebound is found to occur

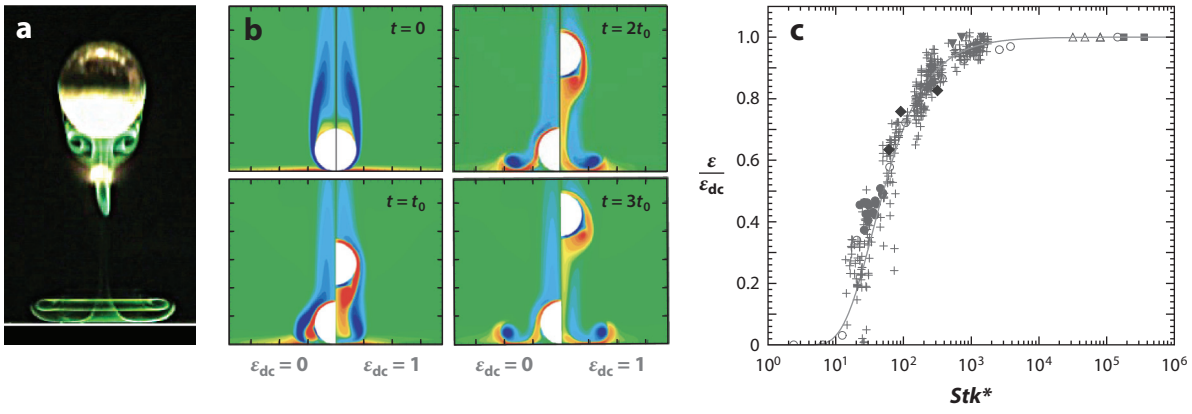


**Figure 21**

Rebound of a sphere of diameter $D$ from a wall after impact from a distance $L$. (*a*) Forced rebound for $L/D = 5$, $Re = 800$, and dry-collision coefficient of restitution $\varepsilon_{dc} = 1$. Dye visualization in water. Panel *a* reprinted with permission from Thompson et al. (2007), copyright 2007 Cambridge University Press. (*b*) Rebound after a free fall under gravity for $L/D = 5$ and $Re = 865$ (at impact). Vorticity contours from numerical simulations, comparing the cases of plastic ($\varepsilon_{dc} = 0$; left half of the images) and elastic ($\varepsilon_{dc} = 1$; right half) collisions. The timescale is given by $t_0 = 0.8\sqrt{D/g}$ ($g$ is gravitational acceleration). (*c*) Normalized coefficient of restitution $\varepsilon/\varepsilon_{dc}$ as function of modified Stokes number $Stk^*$, collected from various studies. Panels *b*,*c* adapted with permission from Ardekani & Rangel (2008), copyright 2008 Cambridge University Press.

below a critical value of $Stk^* \approx 10$, and the coefficient of restitution approaches that for a dry collision ($\varepsilon_{dc}$) for $Stk^* \gtrsim 1{,}000$, as shown in **Figure 21*c***.

As for rolling bodies discussed in Sections 4.2 and 4.3 above, the issue of whether there is solid-to-solid contact, or whether lubrication forces prevent this contact, is relevant also to a bluff-body impact and rebound. In the study by Davis et al. (1986), the pressure forces in the viscous liquid lubrication film between the particle and the wall during the collision were found to be sufficiently large to cause the particles to deform elastically and rebound. The Stokes number dependence has been attributed to the drainage of the lubrication film. In this model of elastohydrodynamic collisions based on lubrication theory, the two solids never touch.

Effects that lead to a breakdown of the lubrication approach include, again, surface roughness (Smart & Leighton 1989). Davis (1987) already suggested that when the gap between the surfaces becomes equal to the size of the largest surface roughness element, solid-to-solid contact of the roughness bumps could occur due to the discrete molecular nature of the fluid or attractive London–van der Waals forces. More recently, Birwa et al. (2018) studied the collision between spheres and a wall in a viscous fluid, focusing on the question of solid-to-solid contact. For Stokes numbers below the rebound threshold, the lubrication film forces were found to decelerate the spheres to zero velocity before reaching the wall. As soon as rebound occurred for increasing Stokes numbers, contact between the two solids was systematically detected. The explanation provided was that the lubrication film thickness needed to produce the force for stopping the sphere motion is significantly smaller than the roughness of the particle or the wall, and therefore contact is made via the roughness elements.

## 6. CONCLUDING REMARKS

In this review, we discuss the effect of a wall on the wake structures and transitions of bluff bodies moving relative to the wall. The review is restricted to the generic 2D and 3D bluff bodies—the

## INTERACTION WITH A FREE SURFACE

There are many important interactions that take place at free, or nearly free, surfaces, such as those in oceans, lakes, and rivers, as well as industrial processes involving risers, bridge piers, mixing vessels, and bioreactors. Several studies have provided valuable insights into the surprising wake structures and free-surface response for nonrotating submerged or semisubmerged cylinders or spheres (Sheridan et al. 1997; Kawamura et al. 2002; Chaplin & Teigen 2003; Reichl et al. 2003, 2005; Koo et al. 2004; Vlachos & Tellionis 2008; Shao et al. 2013; Sareen et al. 2018). Far from being a passive boundary, the free surface, when distorted, becomes a rich source of vorticity that can remarkably change the wake of a bluff body (Brøns et al. 2014, Terrington et al. 2020). However, the effects of the interface on the force distribution on the body, vortex generation and turbulence structures, and air–water interface structures still require much further study.



circular cylinder and the sphere, respectively—and to the ambient fluid being at rest relative to the wall. This excludes the class of flows for which boundary layers form due to the fluid flow along the wall and where the bluff body is fixed to the wall, such as is typical in wind engineering applications. The simplified flow allows a clearer analysis of the direct effect that the wall itself has on the wakes. We also consider only interactions with a rigid wall; the sidebar titled Interaction with a Free Surface briefly addresses the configuration of bluff bodies placed near a fluid–fluid interface.

## SUMMARY POINTS

1. Proximity to a wall changes the bluff-body wake structures and transitions significantly. For example, the strong absolute instability causing Bénard–von Kármán vortex shedding for an isolated cylinder becomes much weaker in the immediate presence of a wall, with a predominately single-sided wake, and a steady 3D transition mode appears at higher Reynolds numbers.
2. Flow underneath a cylinder or sphere is restricted as the body is moved closer to the wall, which effectively eliminates shedding of near-wall vortices. However, the proximity of the upper shed vortices to the wall leads to secondary vorticity generation there, which can roll up into discrete structures forming pairs with the upper vortex. These pairs propagate away from the wall, causing a significant spread of the wake. This mechanism dominates the flow dynamics for the cylinder case, but is less important for a sphere.
3. For small gaps (less than 1% of the body diameter), the gap flow effectively becomes uncoupled from the global flow around rolling bodies, hence simulations of rolling bodies with small imposed gaps produce wake dynamics relatively insensitive to the gap ratio. However, this is not true for the lift and especially the drag forces, which are very sensitive to gap size.
4. The flow dynamics for bluff bodies impacting a surface is governed by the starting distance and the Reynolds number. A vortex system is formed from the initial wake (vortex pair for the cylinder, vortex ring for the sphere) and secondary wall vorticity, which propagates away from the impact point. At higher Reynolds numbers, it becomes three-dimensionally unstable through an elliptic instability in the case of a cylinder, and a centrifugal-type instability for the sphere.

5. For freely rolling or sliding bodies, surface roughness appears to be a key element, leading to an effective contact between the two solids, while at the same time providing an effective finite gap. Predicted drag coefficients for smooth spheres rolling without slip are similar to those observed in experiments for a roughness height on the order of the chosen gap size. However, this requires further investigation.

## FUTURE ISSUES

1. Studies of the wakes of sliding and rolling bodies of other geometries (elliptical cylinders, cubes) and the combined wakes of multiple bodies, particularly spheres, in motion near walls will extend current knowledge to a broader set of applications.
2. Simulations of rolling/sliding bodies near surfaces at higher Reynolds numbers are required to examine turbulent transition and fully turbulent wakes.
3. The effects of body rotation, as well as wall and body material elasticity, on the wakes of impacting bluff bodies are largely unexplored.
4. The details of the physics of solid-to-solid contact due to surface roughness need to be further addressed, ideally through a combination of careful experiments, detailed numerical simulations resolving the flow near the gap, and theoretical analysis.
5. How bluff bodies interact with free surfaces and multifluid interfaces is yet to be investigated in detail.



## DISCLOSURE STATEMENT

The authors are not aware of any factors that might be perceived as affecting the objectivity of this review.

## ACKNOWLEDGMENTS

We wish to acknowledge generous support from the Australian Research Council through Discovery Project grants DP130100822, DP150102879, DP170100275, and DP200100704. M.C.T. and K.H. also acknowledge generous computing allocations from the National Computing Infrastructure (Canberra) and Pawsey Supercomputing Centre (Perth) through grants n67 and d71.

## LITERATURE CITED

Ardekani AM, Rangel H. 2008. Numerical investigation of particle–particle and particle–wall collisions in a viscous fluid. *J. Fluid Mech.* 596:437–66

Ashmore J, del Pino C, Mullin T. 2005. Cavitation in a lubrication flow between a moving sphere and a boundary. *Phys. Rev. Lett.* 94:124501

Barkley D, Henderson RD. 1996. Three-dimensional Floquet stability analysis of the wake of a circular cylinder. *J. Fluid Mech.* 322:215–41

Bearman PW. 1984. Vortex shedding from oscillating bluff bodies. *Annu. Rev. Fluid Mech.* 16:195–222

Berger E, Wille R. 1972. Periodic flow phenomena. *Annu. Rev. Fluid Mech.* 4:313–40

Birwa SK, Rajalakshmi G, Govindarajan R. 2018. Solid-on-solid contact in a sphere-wall collision in a viscous fluid. *Phys. Rev. Fluids* 3:004302

Bourguet R, Lo Jacono D. 2014. Flow-induced vibrations of a rotating cylinder. *J. Fluid Mech.* 740:342–80

Brändle de Motta JC, Breugem W-P, Gazanion B, Estivalezes J-L, Vincent S, Climent E. 2013. Numerical modelling of finite-size particle collisions in a viscous fluid. *Phys. Fluids* 25:083302

Brennen CE. 1982. *A review of added mass and fluid inertial forces*. Tech. Rep. N62583-81-MR-554, Naval Civil Eng. Lab., Port Hueneme, CA

**Lubrication theory for a sphere impacting on a wall.**

**Brenner H. 1961. The slow motion of a sphere through a viscous fluid towards a plane surface. *Chem. Eng. Sci.* 16:242–51**

Brøns M, Thompson MC, Leweke T, Hourigan K. 2014. Vorticity generation and conservation for two-dimensional interfaces and boundaries. *J. Fluid Mech.* 758:63–93

Brücker C. 2001. Spatio-temporal reconstruction of vortex dynamics in axisymmetric wakes. *J. Fluids Struct.* 5:543–54

Carty JJ. 1957. *Resistance coefficients for spheres on a plane boundary*. BSc Thesis, MIT, Cambridge, MA

Chaplin JR, Teigen P. 2003. Steady flow past a vertical surface-piercing circular cylinder. *J. Fluids Struct.* 18:271–85

Cherukat P, McLaughlin JB. 1994. The inertial lift on a rigid sphere in a linear shear flow field near a flat wall. *J. Fluid Mech.* 263:1–18

Chomaz JM, Bonneton P, Hopfinger EJ. 1993. The structure of the near wake of a sphere moving horizontally in a stratified fluid. *J. Fluid Mech.* 254:1–21

Choi H, Jeon W-P, Kim J. 2008. Control of flow over a bluff body. *Annu. Rev. Fluid Mech.* 40:113–19

Clark HM. 1992. The influence of the flow field in slurry erosion. *Wear* 152:223–40

**Along with Davis et al. (1986): elastohydrodynamic modeling of sphere rebound.**

**Davis RH. 1987. Elastohydrodynamic collisions of particles. *PCH Physicochem. Hydrodyn.* 9:41–52**

Davis RH, Serayssol JM, Hinch EJ. 1986. The elastohydrodynamic collision of two spheres. *J. Fluid Mech.* 163:479–97

Dobson J, Ooi A, Poon EKW. 2014. The flow structures of a transversely rotating sphere at high rotation rates. *Comput. Fluids* 102:170–81

Dušek J, Le Gal P, Fraunié P. 1994. A numerical and theoretical study of the first Hopf bifurcation in a cylinder wake. *J. Fluids Mech.* 264:59–80

Eames I, Dalziel SB. 1999. Resuspension by an impacting sphere. *Phys. Fluids* 11:S11

Ern P, Risso F, Fabre D, Magnaudet J. 2012. Wake-induced oscillatory paths of bodies freely rising or falling in fluids. *Annu. Rev. Fluid Mech.* 44:97–121

Galilei G. 1914 (1638). *Dialogues Concerning Two New Sciences*, transl. H Crew, A de Salvio. New York: Macmillan

Galvin KP, Zhao Y, Davis RH. 2001. Time-averaged hydrodynamic roughness of a non-colloidal sphere in low Reynolds number motion down an inclined plane. *Phys. Fluids A* 13:3108–9

Garde RJ, Sethuraman S. 1969. Variation of the drag coefficient of a sphere rolling along a boundary. *Houille Blanche* 7:727–32

Ghidersa B, Dušek J. 2000. Breaking of axisymmetry and onset of unsteadiness in the wake of a sphere. *J. Fluid Mech.* 423:33–69

Giacobello M, Ooi A, Balachandar S. 2009. Wake structure of a transversely rotating sphere at moderate Reynolds numbers. *J. Fluid Mech.* 621:103–30

**Lubrication theory for a sphere moving along a wall.**

**Goldman AJ, Cox RG, Brenner H. 1967. Slow viscous motion of a sphere parallel to a plane wall—I. Motion through a quiescent fluid. *Chem. Eng. Sci.* 22:637–51**

Gondret P, Hallouin E, Lance M, Petit L. 1999. Experiments on the motion of a solid sphere toward a wall: from viscous dissipation to elasto-hydrodynamic bouncing. *Phys. Fluids* 11:2803–5

Gondret P, Lance M, Petit L. 2002. Bouncing motion of spherical particles in fluids. *Phys. Fluids* 14:643–52

He W, Gioria R, Pérez J, Theofilis V. 2017. Linear instability of low Reynolds number massively separated flow around three NACA airfoils. *J. Fluid Mech.* 811:701–41

Henderson RD. 1997. Nonlinear dynamics and pattern formation in turbulent wake transition. *J. Fluid Mech.* 353:65–112

Houdroge FY, Leweke T, Hourigan K, Thompson MC. 2017. Two- and three-dimensional wake transitions of an impulsively started uniformly rolling circular cylinder. *J. Fluid Mech.* 826:32–59

Houdroge FY, Leweke T, Hourigan K, Thompson MC. 2020. Wake dynamics and flow-induced vibration of a freely rolling cylinder. *J. Fluid Mech.* 903:A48
Huang WX, Sung HJ. 2007. Vortex shedding from a circular cylinder near a moving wall. *J. Fluids Struct.* 23:1064–76
Hunt JCR, Wray AA, Moin P. 1988. Eddies, streams, and convergence zones in turbulent flows. In *Center for Turbulence Research Proceedings of the Summer Program 1988*, pp. 193–208. Stanford, CA: Cent. Turbul. Res.
Jan C-D, Shen H-W. 1995. Drag coefficients for a sphere rolling down an inclined channel. *J. Chin. Inst. Eng.* 18:493–507
Jeong J, Hussain F. 1995. On the identification of a vortex. *J. Fluid Mech.* 285:69–94
Johnson TA, Patel VC. 1999. Flow past a sphere up to a Reynolds number of 300. *J. Fluid Mech.* 378:19–70
Joseph GG, Zenit R, Hunt ML, Rosenwinkel AM. 2001. Particle–wall collisions in a viscous fluid. *J. Fluid Mech.* 433:329–46
Kawamura T, Mayer S, Garapon A, Sorensen L. 2002. Large eddy simulation of a flow past free surface piercing circular cylinders. *ASME J. Fluids Eng.* 124:91–101
Kerswell RR. 2002. Elliptical instability. *Annu. Rev. Fluid Mech.* 34:83–113
Kim D. 2009. Laminar flow past a sphere rotating in the transverse direction. *J. Mech. Sci. Technol.* 23:578–89
King MR, Leighton DT Jr. 1997. Measurement of the inertial lift on a moving sphere in contact with a plane wall in a shear flow. *Phys. Fluids* 9:1248–55
Koo B, Yang J, Yeon SM, Stern F. 2004. Reynolds and Froude number effect on the flow past an interface-piercing circular cylinder. *Int. J. Nav. Archit. Ocean Eng.* 6:529–61
Lecoq N, Anthore R, Cichocki K, Szymczak P, Feuillebois F. 2004. Drag force on a sphere moving towards a corrugated wall. *J. Fluid Mech.* 513:247–64
Legendre D, Daniel C, Guiraud P. 2005. Experimental study of a drop bouncing on a wall in a liquid. *Phys. Fluids* 17:097105
Leweke T, Le Dizès S, Williamson CHK. 2016. Dynamics and instabilities of vortex pairs. *Annu. Rev. Fluid Mech.* 48:507–41
Leweke T, Schouveiler L, Thompson MC, Hourigan K. 2008. Unsteady flow around impacting bluff bodies. *J. Fluids Struct.* 24:1194–203
Leweke T, Thompson MC, Hourigan K. 2004a. Touchdown of a sphere. *Phys. Fluids* 16:S5
Leweke T, Thompson MC, Hourigan K. 2004b. Vortex dynamics associated with the collision of a sphere with a wall. *Phys. Fluids* 16:L74–77
Leweke T, Thompson MC, Hourigan K. 2006. Instability of the flow around an impacting sphere. *J. Fluids Struct.* 22:961–71
Li X, Hunt ML, Colonius T. 2012. A contact model for normal immersed collisions between a particle and a wall. *J. Fluid Mech.* 691:123–45
Lian G, Adams MJ, Thornton C. 1996. Elastohydrodynamic collisions of solid spheres. *J. Fluid Mech.* 311:141–52
Lim TT. 1989. An experimental study of a vortex ring interacting with an inclined wall. *Exp. Fluids* 7:453–63
Lim TT, Nichols TB, Chong MS. 1991. A note on the cause of the rebound in the head-on collision of a vortex ring with a wall. *Exp. Fluids* 12:41–48
Magarvey RH, Bishop RL. 1961a. Transition ranges for three-dimensional wakes. *Can. J. Phys.* 39:1418–22
Magarvey RH, Bishop RL. 1961b. Wakes in liquid-liquid systems. *Phys. Fluids* 4:800–5
Masuda N, Yoshida J, Ito B, Furuya T, Sano O. 2012. Collision of a vortex ring on granular material. Part I. Interaction of the vortex ring with the granular layer. *Fluid Dyn. Res.* 44:015501
**Merlen A, Frankiewicz C. 2011. Cylinder rolling on a wall at low Reynolds numbers. *J. Fluid Mech.* 685:461–94**
Mittal R. 1999. Planar symmetry in the unsteady wake of a sphere. *AIAA J.* 37:388–90
Mittal S, Kumar B. 2003. Flow past a rotating cylinder. *J. Fluid Mech.* 476:303–34
Oertel H. 1990. Wakes behind blunt bodies. *Annu. Rev. Fluid Mech.* 22:539–64

**Lubrication theory for a cylinder moving along a wall.**

Orlandi P, Verzicco R. 1993. Vortex rings impinging on walls: axisymmetric and three-dimensional simulations. *J. Fluid Mech.* 256:615–46

Poon EKW, Ooi ASH, Giacobello M, Iaccarino G, Chung D. 2014. Flow past a transversely rotating sphere at Reynolds numbers above the laminar regime. *J. Fluid Mech.* 759:751–81

Pralits JO, Brandt L, Giannetti F. 2010. Instability and sensitivity of the flow around a rotating circular cylinder. *J. Fluid Mech.* 650:513–36

Prasad A, Williamson CHK. 1997. The instability of the shear layer separating from a bluff body. *J. Fluid Mech.* 333:375–402

Prokunin AN. 2003. On a paradox in the motion of a rigid particle along a wall in a fluid. *Fluid Dyn.* 38:443–57

Prokunin AN. 2004. Microcavitation in the slow motion of a solid spherical particle along a wall in a fluid. *Fluid Dyn.* 39:771–78

Rajamuni MM, Thompson MC, Hourigan K. 2018. Vortex-induced vibration of a transversely rotating sphere. *J. Fluid Mech.* 847:786–820

Rao A, Passaggia P-Y, Bolnot H, Thompson MC, Leweke T, Hourigan K. 2012. Transition to chaos in the wake of a rolling sphere. *J. Fluid Mech.* 695:135–48

Rao A, Radi A, Leontini J, Thompson MC, Sheridan J, Hourigan K. 2015a. A review of rotating cylinder wake transitions. *J. Fluids Struct.* 53:2–14

Rao A, Stewart BE, Thompson MC, Leweke T, Hourigan K. 2011. Flows past rotating cylinders next to a wall. *J. Fluids Struct.* 27:668–79

Rao A, Thompson MC, Leweke T, Hourigan K. 2013. The flow past a circular cylinder translating at different heights above a wall. *J. Fluids Struct.* 41:9–21

**Rao A, Thompson MC, Leweke T, Hourigan K. 2015b. Flow past a rotating cylinder translating at different gap heights along a wall. *J. Fluids Struct.* 57:314–30**

Reichl P, Hourigan K, Thompson MC. 2003. The unsteady wake of a circular cylinder near a free surface. *Flow Turbul. Combust.* 71:347–59

Reichl P, Hourigan K, Thompson MC. 2005. Flow past a cylinder close to a free surface. *J. Fluid Mech.* 533:269–96

Robichaux J, Balachandar S, Vanka SP. 1999. Three-dimensional Floquet instability of the wake of square cylinder. *Phys. Fluids A* 11:560–78

Ruiz-Angulo A, Hunt ML. 2010. Measurements of the coefficient of restitution for particle collisions with ductile surfaces in a liquid. *Granul. Matter* 12:185–91

Sareen A, Zhao J, Sheridan J, Hourigan K, Thompson MC. 2018. Vortex-induced vibrations of a sphere close to a free surface. *J. Fluid Mech.* 846:1023–58

Seddon JRT, Mullin T. 2006. Reverse rotation of a cylinder near a wall. *Phys. Fluids* 18:041703

Shao Y, Zhang Y-P, Zhu DZ, Zhang T-Q. 2013. Drag force on a free surface-piercing yawed circular cylinder in steady flow. *J. Fluids Struct.* 43:145–63

Sheard GJ. 2011. Wake stability features behind a square cylinder: focus on small incidence angles. *J. Fluids Struct.* 27:734–42

Sheard GJ, Leweke T, Thompson MC, Hourigan K. 2007. Flow around an impulsively arrested circular cylinder. *Phys. Fluids* 19:083601

Sheard GJ, Thompson MC, Hourigan K, Leweke T. 2005. The evolution of a subharmonic mode in a vortex street. *J. Fluid Mech.* 534:23–38

Sheridan J, Lin J-C, Rockwell D. 1997. Flow past a cylinder close to a free surface. *J. Fluid Mech.* 330:269–96

Smart JR, Beimfohr S, Leighton DT. 1993. Measurement of the translational and rotational velocities of a non-colloidal sphere rolling down a smooth inclined plane at low Reynolds number. *Phys. Fluids A* 5:13–24

Smart JR, Leighton DT. 1989. Measurement of the hydrodynamic surface roughness of non-colloidal spheres. *Phys. Fluids A* 1:52–60

Stewart BE. 2008. *The dynamics and stability of flows around rolling bluff bodies*. PhD Thesis, Monash Univ./Univ. Provence Aix-Marseille I, Melb., Aust./Marseille, Fr.

Stewart BE, Hourigan K, Thompson MC, Leweke T. 2006. Flow dynamics and forces associated with a cylinder rolling along a wall. *Phys. Fluids* 18:111701

**Survey of cylinder wake instability modes as function of rotation rate and wall proximity [Rao et al. (2015a) provide the case without a wall].**

Stewart BE, Leweke T, Hourigan K, Thompson MC. 2008. Wake formation behind a rolling sphere. *Phys. Fluids* 20:071704
Stewart BE, Thompson MC, Leweke T, Hourigan K. 2010a. Numerical and experimental studies of the rolling sphere wake. *J. Fluid Mech.* 643:137–62
Stewart BE, Thompson MC, Leweke T, Hourigan K. 2010b. The wake behind a cylinder rolling on a wall at varying rotation rates. *J. Fluid Mech.* 648:225–56
Stojković D, Breuer M, Durst F. 2002. Effect of high rotation rates on the laminar flow around a circular cylinder. *Phys. Fluids* 14:3160–78
Stojković D, Schön P, Breuer M, Durst F. 2003. On the new vortex shedding mode past a rotating circular cylinder. *Phys. Fluids* 15:1257–60
Swearingen JD, Crouch JD, Handler RA. 2000. Dynamics and stability of a vortex ring impacting a solid boundary. *J. Fluid Mech.* 297:1–28
**Taneda S. 1965. Experimental investigation of vortex streets. *J. Phys. Soc. Jpn.* 20:1714–21**
Tatsuno M, Taneda S. 1971. Visualization of the unsteady flow past cylinders and plates decelerated from a steady speed. *J. Phys. Soc. Jpn.* 31:1266–74
Taylor GI. 1963. Cavitation of a viscous fluid in narrow passages. *J. Fluid Mech.* 16:595–619
Terrington SJ, Hourigan K, Thompson MC. 2020. The generation and conservation of vorticity: deforming interfaces and boundaries in two-dimensional flows. *J. Fluid Mech.* 890:A5
Thompson MC, Hourigan K. 2005. The shear layer instability of a circular cylinder wake. *Phys. Fluids* 17:021702
Thompson MC, Hourigan K, Cheung, Leweke T. 2006a. Hydrodynamics of a particle impact on a wall. *Appl. Math. Mod.* 30:1356–69
Thompson MC, Hourigan K, Ryan K, Sheard GJ. 2006b. Wake transition of two-dimensional cylinders and axisymmetric bluff bodies. *J. Fluids Struct.* 22:793–806
Thompson MC, Hourigan K, Sheridan J. 1996. Three-dimensional instabilities in the wake of a circular cylinder. *Exp. Therm. Fluid Sci.* 12:190–96
**Thompson MC, Leweke T, Hourigan K. 2007. Sphere-wall collisions: vortex dynamics and stability. *J. Fluid Mech.* 575:121–48**
Thompson MC, Leweke T, Provansal M. 2001. Kinematics and dynamics of sphere wake transition. *J. Fluid Struct.* 15:575–86
Tomboulides AG, Orszag SA. 2000. Numerical investigation of transitional and weak turbulent flow past a sphere. *J. Fluid Mech.* 416:45–73
Verekar PK, Arakeri JH. 2010. Sphere rolling down an incline submerged in a liquid. In *Proceedings of the 37th International and 4th National Conference on Fluid Mechanics and Fluid Power*, Pap. FMFP10-AM-01. Chennai, India: Indian Inst. Technol. Madras
Vlachos PP, Tellionis D. 2004. The effect of free surface on the vortex shedding from inclined circular cylinders. *ASME J. Fluids Eng.* 130:021103
Walker JD, Smith CR, Cerra AW, Doligalski TL. 1987. The impact of a vortex ring on a wall. *J. Fluid Mech.* 181:99–140
Wang W, Dalton C. 1991. Numerical solutions for impulsively started and decelerated viscous flow past a circular cylinder. *Int. J. Numer. Methods Fluids* 12:383–400
Willetts B. 1998. Aeolian and fluvial grain transport. *Philos. Trans. R. Soc. Lond. A* 356:2497–513
Williamson CHK. 1989. Oblique and parallel modes of vortex shedding in the wake of a circular cylinder at low Reynolds numbers. *J. Fluid Mech.* 206:579–627
Williamson CHK. 1996a. Three-dimensional wake transition. *J. Fluid Mech.* 328:345–407
Williamson CHK. 1996b. Vortex dynamics in the cylinder wake. *Annu. Rev. Fluid Mech.* 28:477–539
Williamson CHK, Govardhan R. 2004. Vortex-induced vibrations. *Annu. Rev. Fluid Mech.* 36:413–55
Yildirim B, Yang H, Gouldstone A, Müftü S. 2017. Rebound mechanics of micrometre-scale, spherical particles in high-velocity impacts. *Proc. R. Soc. A* 473:20160936
Yoon H, Lee J, Seo J, Park H. 2010. Characteristics for flow and heat transfer around a circular cylinder near a moving wall in wide range of low Reynolds number. *Int. J. Heat Mass Transf.* 53:5111–20
Zeng L, Balachandar S, Fischer P. 2005. Wall-induced forces on a rigid sphere at finite Reynolds number. *J. Fluid Mech.* 536:1–25

**First visualization of the wake of a cylinder moving parallel to a wall.**

**Comprehensive study of the flow generated by the wall impact of a sphere.**

Zeng L, Najjar F, Balachandar S, Fischer P. 2009. Forces on a finite-sized particle located close to a wall in a linear shear flow. *Phys. Fluids* 21:033302

Zhao J, Lo Jacono D, Sheridan J, Hourigan K, Thompson MC. 2018. Experimental investigation of in-line flow-induced vibration of a rotating circular cylinder. *J. Fluid Mech.* 847:664–99

Zhao Y, Galvin KP, Davis RH. 2002. Motion of a sphere down a rough plane in a viscous fluid. *Int. J. Multiph. Flow* 28:1787–800

Ziskind G. 2006. Particle resuspension from surfaces: revisited and re-evaluated. *Rev. Chem. Eng.* 22:1–123

Annual Review of Fluid Mechanics

Volume 53, 2021

# Contents

**Indexes**



**Errata**

An online log of corrections to *Annual Review of Fluid Mechanics* articles may be found at http://www.annualreviews.org/errata/fluid